



Data-driven estimates of evapotranspiration and its drivers in the Congo Basin

Michael W. Burnett¹, Gregory R. Quetin², Alexandra G. Konings²

¹Earth Systems Program, Stanford University, Stanford, CA, USA

5 ²Department of Earth System Science, Stanford University, Stanford, CA, USA

Correspondence to: Michael W. Burnett (mburnett@alumni.stanford.edu)

Abstract

Evapotranspiration (ET) from tropical forests serves as a critical moisture source for regional and global climate cycles. However, the magnitude, seasonality, and interannual variability of ET in the Congo Basin remain poorly constrained due to a scarcity of direct observations, despite it being the second-largest river basin the world and containing a vast region of tropical forest. In this study, we applied a water balance model to an array of remotely-sensed and in-situ datasets to produce monthly, basin-wide ET estimates spanning April 2002 to November 2016. Data sources include water storage changes estimated from the Gravity Recover and Climate Experiment (GRACE) satellites, in-situ measurements of river discharge, and precipitation from several remotely sensed sources. An optimal precipitation dataset was determined as a weighted average of interpolated data by Nicholson et al. (2018), Climate Hazards Infrared Precipitation with Station Version 2 (CHIRPS2) data, and the Precipitation Estimation from Remotely Sensed Information using Artificial Neural Networks–Climate Data Record product (PERSIANN–CDR), with the relative weights based on the error magnitudes in each dataset as determined by triple collocation. The resulting water balance-derived ET (ET_{wb}) features a long-term average that is consistent with previous studies (117.2±3.5 cm/year), but displays greater seasonal and interannual variability than six global ET products. The seasonal cycle of ET_{wb} generally tracks that of precipitation over the basin, with the exception that ET_{wb} is greater in March–April–May (MAM) than in the relatively wetter September–October–November (SON) periods. This pattern appears to be driven by seasonal variations in diffuse photosynthetically-active radiation (PAR) fraction, net radiation (R_n), and soil water availability. From 2002–2016, R_n , PAR, and vapor-pressure deficit (VPD) all increase significantly within the Congo Basin; however, no corresponding trend occurred in ET_{wb} . We hypothesize that the stability of ET_{wb} over the study period despite sunnier and less humid conditions is likely due to increasing atmospheric CO₂ concentrations that offset the impacts of rising VPD and irradiance on stomatal water use efficiency (WUE).

1 Introduction

The Congo River Basin in central Africa is the second-largest river basin in the world and supports one of Earth's three major humid tropical forest regions (Alsdorf et al., 2016). Approximately 24 to 39 percent of evapotranspiration (ET) from the Congo



30 Basin is recycled as local rainfall (Dyer et al., 2017), and model simulations indicate changes in ET within the basin affect
moisture cycling across the African continent (Van Der Ent and Savenije, 2011; Bell et al., 2015; Sorí et al., 2017).
Understanding the magnitude, variability, and drivers of ET in the Congo Basin is therefore crucial for studying the climate
systems of central Africa and the global tropics, especially because significant environmental shifts have already been reported
within the basin. For instance, deforestation is an ongoing problem in Congolese forests, with potential impacts on climate
35 (Laporte et al., 2007; Batra et al., 2008; Bell et al., 2015; Turubanova et al., 2018); temperatures are rising due to anthropogenic
climate change (James and Washington, 2013); and many have reported a long-term decline in precipitation over the basin
(Asefi-Najafabady and Saatchi, 2013; Diem et al., 2014; Zhou et al., 2014; Hua et al., 2016; Dezfuli, 2017). Such shifts are
particularly concerning because Africa's tropical rainforests are already significantly drier than other humid tropical forests
and exist at the threshold of conversion from evergreen to deciduous trees (Guan et al., 2015; Philippon et al., 2019).

40 However, the hydrology of the Congo Basin is vastly understudied relative to the region's size and influence (Alsdorf
et al., 2016). In particular, no long-term observational studies of ET in the basin exist. There are also no eddy covariance
towers operating within the Congo Basin. Prior studies provide only limited information and either analyze short-term (<1
month) ET observations at individual site scale (Nizinski et al., 2011, 2014) or rely on combining meteorological measurements
45 to evaluate regional-scale ET (Matsuyama et al., 1994; Shem, 2006; Batra et al., 2008; Chishugi and Alemaw, 2009; Marshall
et al., 2012; Ndehedehe et al., 2018; Crowhurst et al., 2020). However, the large size and heterogeneity of the Congo Basin
render point-based approaches inadequate for basin-scale analysis of hydrological cycling, and regional scale models suffer
from being poorly constrained because of the widespread lack of in-situ observations throughout the basin (e.g. little
understanding of local variability in rooting depth, vegetation responses to water and light availability, canopy interception,
50 etc.). As a result, even basic seasonality patterns across the Congo Basin remain unclear. For example, Konings et al. (2017)
showed that canopy water content increases during dry season, which could be due to either dry season leaf-out or a change in
plant water uptake during the dry season that would increase ET. The latter could not be ruled out in Konings et al. (2017) due
to the lack of direct ET estimates in the region.

Remote sensing offers a partial solution to this scarcity of ET observations. Remote sensing-based estimates of ET
55 are generally indirect, relying on physical models to link temperature, meteorological inputs, and/or other observables to the
rate of ET (Zhang et al., 2016). However, these global modeling approaches are poorly constrained in the Congo River Basin
and may be highly erroneous there. Alternatively, basin-scale ET can be estimated indirectly by inverting the water balance.
This approach requires only three geophysical input variables: precipitation, river discharge, and the change in terrestrial water
storage. Precipitation and total water storage change can both be estimated using remote sensing, with the latter determined by
60 gravity measurements from the Gravity Recovery and Climate Mission (GRACE) (Tapley et al., 2004; Swenson, 2012). Recent
examples of this method's application include the Amazon Basin (Maeda et al., 2017; Swann and Koven, 2017) and the
coterminous United States (Wan et al., 2015), as well as global examinations of basin-scale ET (Liu et al., 2016). While some
previous studies have applied a similar technique to the Congo Basin as part of larger-scale studies, these studies assumed



terrestrial water storage was constant over their study periods (Marshall et al., 2012; Ukkola and Prentice, 2013; Weerasinghe
65 et al., 2020)—an assumption with little support. Indeed, remotely-sensed evidence suggests water storage anomalies within
the basin do change significantly on monthly and interannual timescales (Crowley et al., 2006; Rodell et al., 2018). In this
paper, we applied the water balance method to the Congo Basin to produce the first data-driven estimates of monthly basin-
averaged ET for the period from April 2002 to November 2016. To determine the most accurate precipitation time series to
use in this computation, precipitation estimated from multiple remote sensing-based approaches are combined based on
70 uncertainty estimation using triple collocation. We further used the resulting ET time series to explore the climatic and
ecological drivers of ET seasonality and trends by comparing it against a variety of vegetation indices and meteorological
drivers.

2 Methods

Based on mass balance, any precipitation that falls on a basin and is not removed from the basin through river discharge or ET
75 must increase the amount of water stored in the basin in the form of groundwater, soil moisture, or open water bodies. The
equation for this mass balance can be rearranged to solve for ET as follows:

$$ET_{wb} = P - Q - \frac{dS}{dt} \quad (1)$$

where ET_{wb} is monthly basin-wide evapotranspiration, P is the monthly basin-wide precipitation, Q is total monthly runoff
from the Congo River, S is the water storage anomaly within the basin expressed as an equivalent water height (Rodell et al.,
80 2004a, 2011), and t is time. We calculate ET_{wb} using P from a combination of remotely-sensed and gauge-based precipitation
products, as further discussed in Sects. 2.1 and 2.2. Q was obtained from a stream gauge at the outlet of the Congo River at
Kinshasa-Brazzaville. Lastly, dS/dt was derived from the monthly change in terrestrial water storage throughout the basin, as
estimated by gravitational anomaly data from GRACE (Tapley et al., 2004; Swenson, 2012).

2.1 Water balance data sources

85 The area and extent of the Congo Basin were determined using the 15-arcsecond HydroSHEDS Level 5 Basin Boundaries
product (Lehner et al., 2008). The HydroSHEDS boundary produces a total basin area of 3,705,220 km²—in good agreement
with a recent independent estimate of 3,687,000 km² (Alsdorf et al., 2016). The HydroSHEDS product was used to trim all
remotely-sensed raster data to the Congo Basin's boundaries at 0.01° spatial resolution (all datasets with coarser spatial
resolutions mentioned hereafter were first resampled to 0.01° grids with no interpolation before determining their basin-wide
90 values).

Basin-wide runoff (Q) for the Congo Basin was estimated using monthly discharge data collected from the Congo
River at Kinshasa-Brazzaville. The long-running gauging station is operated by the Observation Service for Geodynamical,
Hydrological and Biogeochemical Control of Erosion/Alteration and Material Transport in the Amazon, Orinoco and Congo



Basins (SO-HYBAM) and captures the drainage of over 98% of the Congo Basin's area (Alsdorf et al., 2016). Because no
95 uncertainty estimate is available for the streamflow gauge, we assumed an uncertainty range of $\pm 20\%$.

Changes in terrestrial water storage (dS/dt) were calculated using S data from NASA's Gravity Recovery and Climate
Experiment (GRACE) satellites (Swenson and Wahr, 2006; Landerer and Swenson, 2012; Swenson, 2012). In order to estimate
monthly S , three independent GRACE solutions in 1° grids from Geoforschungs Zentrum Potsdam (GFZ), Jet Propulsion
Laboratory (JPL), and the Center for Space Research at University of Texas, Austin (CSR) were retrieved. A scale factor grid
100 was also applied to the GRACE data to account for attenuation of small-scale surface mass variations (Landerer and Swenson,
2012). The arithmetic mean of the three S solutions was used in the primary dS/dt calculation in order to reduce noise (Wahr
et al., 2006; Sakumura et al., 2014), though all three independent S solutions were also used to calculate unique dS/dt values
in order to estimate uncertainty in the GRACE products (Lee et al., 2011). The S data were converted to dS/dt values using a
centered-difference approach at monthly timescale:

$$105 \quad \frac{dS}{dt_n} = (S_{n+1} - S_{n-1}) \quad (2)$$

where the S terms are expressed in centimeters of equivalent water height averaged over the entire Congo Basin for the months
before and after month n (Landerer et al., 2010). The uncertainty of dS/dt is calculated as half of the difference between the
highest and lowest dS/dt values from the three GRACE S solutions in any given month (Lee et al., 2011)

Beginning in early 2011, the GRACE mission began an active battery management strategy that resulted in data gaps
110 every several months. In order to reconstruct dS/dt data from 2011–2016, we use its average seasonal cycle to correct for
interannual variability based on the amount of that variability in nearby months. First, the mean monthly cycle of S was
calculated from data-complete months from 2002–2016. For every missing month from 2011–2016, the average S from the
two other months in the same season of the same year (DJF, MAM, JJA, and SON) was compared to the corresponding value
from the multi-year S means. The resulting ratio was then multiplied by the multi-year S mean of the missing month to create
115 the reconstructed S value. Because the sum of multi-year mean S values from October and November is nearly equal to zero
and consequently produces unrealistically-scaled values for September, missing September values were instead interpolated
using August and October of the same year. Repeating the same procedure for months that are available in the GRACE dataset
(i.e. calculating what the reconstructed value would be if it were not available, and comparing it to the observations) shows
that this seasonal-scaling interpolation reproduces true S fairly accurately: from 2002–2016, each of the twelve months was
120 reconstructed with a mean R^2 of 0.75 and a mean root mean square error (RMSE) of 2.80 cm (relative to average seasonal S
variations of ~ 10 cm). Applying this procedure to the mean S data from the three monthly GRACE solutions produced the
complete dS/dt time series that determined the study period for our water balance model (4/2002–11/2016).

Due to the uncertainty of precipitation (P) estimates in the Congo (Washington et al., 2013), P was estimated using
an array of five datasets with different methodologies. These five datasets were chosen because recent validation efforts have
125 shown them to be the most accurate for the Congo Basin (Nicholson et al., 2018, 2019). They include gridded precipitation
data from the Global Precipitation Climatology Centre (GPCC) Version 7.0, which uses interpolation with a worldwide



network of rain gauges to produce monthly precipitation grids (Schneider et al., 2015). GPCP-computed gauges within the Congo are extremely sparse after 2000 (Nicholson et al., 2019), and the GPCP version 7.0 product only lasts through 2013. The Tropical Rainfall Measuring Mission (TRMM) 3B43 Version 7 product (also known as TRMM Multi-Satellite
130 Precipitation Analysis or TMPA), which consists of monthly mean precipitation rate grids, is generated using microwave and infrared sensors on TRMM and other satellites as well as gauge data from the GPCP (Huffman et al., 2007). The Precipitation Estimation from Remotely Sensed Information using Artificial Neural Networks: Climate Data Record (PERSIANN-CDR) product uses satellite infrared data and a neural network approach, calibrated with precipitation forecasts, microwave data, and GPCP gauge data, to produce grids of precipitation estimates at the daily timescale (Ashouri et al., 2015). While PERSIANN
135 is also available without the GPCP gauge corrections that make PERSIANN-CDR so similar to GPCP v7 and TRMM 3B43 over the Congo Basin (Nguyen et al., 2018), it was not used here because it severely overestimates P across Africa (Beighley et al., 2011; Thiemi et al., 2012). Recent studies have found that TRMM Version 7 3B43 and PERSIANN-CDR both perform reasonably well over central Africa (Munzimi et al., 2015; Awange et al., 2016).

Notably, the above three products all depend on GPCP rain gauges to some degree. As a result, all three datasets
140 feature similar rainfall trends and model performance over the Congo Basin during the 2002–2016 period studied here and cannot be considered truly independent P datasets (Nicholson et al., 2019). To that end, the Climate Hazards group Infrared Precipitation with Stations Version 2.0 (CHIRPS2) product, which uses two thermal infrared datasets and interpolated gauge data, was also included as a more independent dataset (Funk et al., 2015). While CHIRPS2 does incorporate some gauge data that overlap with the GPCP product, it is not scaled to fit GPCP data to the same extent as TRMM 3B43 or PERSIANN-CDR
145 are over central Africa (Nicholson et al., 2019)—in fact, the near-total lack of rain gauges within the basin in both CHIRPS2 and GPCP leads to a low correlation between the two datasets within the study area (Funk et al., 2015), indicating the P datasets maintain a high degree of independence. Finally, a recent gauge-based dataset developed for the Congo Basin, NIC131-gridded, served as another independent precipitation data source with coverage through 2014 (Nicholson et al., 2018). The monthly 2.5° NIC131-gridded product was created by applying a spatial reconstruction technique based on principal
150 component analysis to a gauge network that, due to the severe decline of GPCP coverage during the 1990s, is largely independent of the GPCP's gauges in Africa (Nicholson et al., 2019).

2.2 Comparing and unifying precipitation estimates

Because the above five datasets each individually remain highly uncertain, and because no accurate independent basin-wide validation is possible, triple collocation (TC) was used to estimate the error statistics of the different datasets, and ultimately
155 combine them by weighting them according to their relative errors. TC is a method for characterizing systematic and random errors in geophysical measurements using three independent, collocated time series, and even if these datasets are individually noisy (Stoffelen, 1998; McColl et al., 2014). It is particularly valuable in gauge-sparse regions like the Congo Basin because it does not rely on independent error-free validation data. TC-based error calculations have previously been used in a wide variety of geophysical settings—among others, TC was recently used to determine the relative weightings of different



160 hydrologic flux estimates in a neural network-based data combination effort in a manner conceptually analogous to its use here
 (Alemohammad et al., 2017). Rather than the linear model used in most TC applications, we used a multiplicative model that
 is more appropriate for quantifying errors in precipitation estimates (Alemohammad et al., 2015). In the multiplicative error
 model, true precipitation rate T is assumed to be related to the estimated precipitation of product i , P_i , as follows:

$$P_i = a_i T^{\beta_i} e^{\epsilon_i} \quad (3)$$

165 in which a_i is the multiplicative error, β_i is the deformation error, and ϵ_i is the random residual error (which is assumed to have
 zero-mean).

Assuming the three collocated precipitation estimates' residual errors are uncorrelated with each other, and are
 uncorrelated with the true precipitation values, the RMSEs of all three input P datasets may be calculated with Eqs. (4–6):

$$\sigma_{p_1}^2 = C_{11} - \frac{C_{12}C_{13}}{C_{23}} \quad (4)$$

170 $\sigma_{p_2}^2 = C_{22} - \frac{C_{12}C_{23}}{C_{13}} \quad (5)$

$$\sigma_{p_3}^2 = C_{33} - \frac{C_{13}C_{23}}{C_{12}} \quad (6)$$

where C_{ij} is the (i, j) th element of the sample covariance matrix between the three log-transformed datasets and σ_{p_i} is the RMSE
 of the log-transformed P_i time series. σ_{p_i} can be converted to the actual RMSE of P_i by multiplying by the mean value of P_i
 (Alemohammad et al., 2015).

175 The errors of the five P datasets were evaluated by applying TC to triplets of products deemed relatively independent.
 That is, TC was repeated three times using different triplets: TRMM–NIC131–CHIRPS2, GPCC–NIC131–CHIRPS2, and
 PERSIANN–NIC131–CHIRPS2. The three RMSEs calculated for NIC131-gridded and CHIRPS2 were then averaged and
 compared to the RMSEs calculated for TRMM, GPCC, and PERSIANN-CDR. In order to combine the most accurate P time
 series (and their estimated errors) into a single unified P estimate, weighting factors were assigned to each time series in a
 180 manner inversely proportional to the product RMSE. That is, each weighting factor w_i was assigned as in (Eq. 7):

$$w_i = \frac{RMSE_i^{-1}}{\sum_1^3 RMSE_i^{-1}} \quad (7)$$

The best-estimate rate of precipitation for each month was then calculated as a weighted average across all five original
 precipitation products, using w_i . The resulting dataset's RMSE was also used to propagate precipitation uncertainty into the
 uncertainty of ET_{wb} using a root-mean-square sum of the weighted errors. While longer time series are generally preferred for
 185 use in TC in order to reduce sampling error, data prior to 2002 were discarded in the TC analysis because the greater number
 of gauges prior to 2002 likely leads to different error statistics than in this period (Nicholson et al., 2018).

2.3 Comparison to global ET products

Many hydrological studies of the Congo Basin rely on global ET products to constrain their models (e.g. Ndehedehe et al.
 2018; Hassan and Jin 2016). We analyzed six widely-used global ET data products and evaluated their performance relative
 190 to ET_{wb} . MOD16A2 Version 5 is a global ET data product based on the Penman-Monteith equation, meteorological reanalysis,



and remotely-sensed land surface data from the Moderate Resolution Imaging Spectroradiometer (MODIS) satellite mission (Mu et al., 2013). The Global Land Evaporation: Amsterdam Model Version 3.1a (GLEAM v3.1a) product estimates Priestley-Taylor potential ET (PET) from reanalysis radiation and temperature data, then reduces PET to actual ET using remotely sensed soil moisture and vegetation optical depth measurements (Miralles et al., 2011; Martens et al., 2017). Modern-Era
195 Retrospective Analysis for Research and Applications, Version 2 (MERRA-2) is a reanalysis product that integrates a wide variety of observation types from satellites and in-situ sources to produce terrestrial ET estimates using a water balance approach (Gelaro et al., 2017). The Global Land Data Assimilation System Version 2.1 Noah (GLDAS-Noah) product is a land surface simulation forced by a combination of model and observation datasets that provides monthly mean ET estimates (Rodell et al., 2004b).

200 Lastly, two global ET products based on upscaling tower data from global FLUXNET eddy covariance network (Baldocchi et al., 2002) were included: the Model Tree Ensemble (FLUXNET-MTE) product uses a tree-based machine learning approach to upscale carbon, water, and energy flux observations using external global data sources, resulting in a monthly 0.5° global dataset (Jung et al., 2011). The more recent FLUXCOM product uses machine learning algorithms and additional time-varying meteorological inputs to achieve greater accuracy in upscaling flux tower data (Jung et al., 2019). This
205 study uses FLUXCOM's daily RS+METEO version because of its lower ET uncertainty in Africa (Jung et al., 2019). However, it should be noted that FLUXNET-MTE and FLUXCOM, like the physical modeling approaches above, have primarily been validated against observational data in the mid-latitudes. There are no FLUXNET towers located within the Congo basin that could have been used for training these and other models. All datasets were averaged across the Congo basin using linear interpolation.

210 The accuracies of these six products were evaluated by comparing them to the monthly ET_{wb} values: RMSEs, Pearson correlation coefficients, and Taylor skill scores were calculated for each dataset versus ET_{wb} . Only the years 2002–2011 are common to all six ET datasets and the GRACE S data, so all statistics were calculated over this period. Pearson correlation coefficients help determine the ability of each ET model to predict ET_{wb} , while Taylor skill scores allow a comparison of the variability present in each model by accounting for their standard deviations (Taylor, 2001). The average seasonal cycles and
215 interannual variations of the products are also compared to better understand similarities and differences between the products.

2.4 Meteorological and vegetation data

To examine potential drivers of ET's seasonality, interannual variability, and long-term trends in the Congo Basin, ET_{wb} is compared to a host of meteorological and vegetation data including photosynthetically-active radiation (PAR), net radiation (R_n), vapor-pressure deficit (VPD), air and skin temperatures (T_a and T_s), solar-induced fluorescence (SIF), and enhanced
220 vegetation index (EVI). We used all-sky monthly mean PAR and R_n data from the Clouds and the Earth's Radiant Energy System (CERES) project's 1° gridded products. PAR data were derived from the synoptic surface flux model (SYN1deg) (Doelling, 2017), which divides surface PAR fluxes into direct (PAR_{dir}) and diffuse (PAR_{diff}) components, while R_n data were derived from the Energy Balanced and Filled (EBAF) climate data record (Loeb, 2017). The global reanalysis model ERA-



Interim (Dee et al., 2011) provided surface air temperature and relative humidity data in 6-hour increments, which were used
225 to calculate monthly VPD means of the entire basin using linear interpolation. Although reanalysis models over Central Africa
remain uncertain and poorly constrained (Lorenz and Kunstmann, 2012; Brands et al., 2013), these VPD values were tested
against hourly VPD data from Automated Surface Observing Systems (ASOS) and Met Office Integrated Data Archive System
(MIDAS) weather reports from the Congo Basin (Met Office, 2012) and were found to capture monthly cycles of VPD with
acceptable accuracy (Fig. S1).

230 Monthly mean T_a and T_s from the Congo Basin were sourced from the ascending (daytime) retrievals of the
Atmospheric Infrared Sounder (AIRS) Level 3 monthly product (Kahn et al., 2014). The 740 nm SIF data from the Global
Ozone Monitoring Experiment 2 (GOME-2) platform were retrieved from the GOME2_Fluorescence Version 26 Level 3
dataset (Joiner et al., 2013). The GOME-2 SIF dataset is known to have suffered from a significant sensor decay problem
resulting in a spurious worldwide downward trend, so the SIF data were not used in any long-term trend analyses (Zhang et
235 al., 2018). MODIS Collection 6 EVI data processed with the Multi-Angle Implementation of Atmospheric Correction
(MAIAC) algorithm were converted to monthly means from 8-day composite rasters (Huete et al., 2002; Lyapustin et al.,
2018). The MAIAC algorithm, which eliminates errors from aerosols and sun-sensor geometry issues in MODIS data, has
previously proven beneficial for examining vegetation greenness in tropical forests (Hilker et al., 2012; Lyapustin et al., 2012;
Bi et al., 2016). Lastly, annual land cover data from the MODIS-based MCD12C1 Version 6 dataset were retrieved for 2002–
240 2016 and modally-averaged to produce a single land cover classification of the Congo Basin (Friedl and Sulla-Menashe, 2015).
Pixels were aggregated into dominantly deciduous or evergreen vegetation types according to the International Geosphere-
Biosphere Programme's (IGBP) 17-class land cover scheme, with savannas and grasslands considered deciduous and
permanent wetlands considered evergreen. Other vegetation types that are more difficult to generalize (e.g. croplands, mixed
forests, and shrublands) were spatially-limited enough to be ignored once the land cover data were majority-resampled to
245 match the 1° pixel size of our study's coarsest datasets (Fig. S2).

2.5 Removing seasonal cycles and long-term trends

In order to track correlations between ET_{wb} , meteorological variables, and vegetation indices, the Breaks for Additive Season
and Trend (BFAST) R package (Verbesselt et al., 2015) was used to search for abrupt changes in the trends of our time series,
identify linear long-term trends, and remove the average seasonal cycle from the data (Verbesselt et al., 2010a, 2010b).

250 3 Results

3.1 Triple collocation of precipitation datasets

The results of the TC analysis are provided in Table 1. NIC131-gridded exhibited the lowest RMSE in all three
triplets, from 0.60 cm/month to 0.72 cm/month (mean 0.65 cm/month) depending on the triplet. The TC results indicate that
NIC131-gridded, a Congo-specific gauge-based dataset designed using meteorological stations absent from the GPCC network



255 and a principal component-based statistical approach, is the best currently-available P dataset for the Congo Basin after 2002
 (Nicholson et al., 2018). The results in Table 1 agree well with those of Nicholson et al. (2019), which found CHIRPS2 and
 PERSIANN-CDR to be more accurate than TRMM and GPCC in the Congo Basin after 1998. Prior work has also
 demonstrated that CHIRPS2 is among the best P products available for central Africa and outperforms TRMM and
 PERSIANN-CDR on a monthly basis (Dembélé and Zwart, 2016; Nicholson et al., 2019), consistent with the results in Table
 260 1. Given the decreasing availability of Congolese rain gauge data in the GPCC database and the difficulty of measuring P with
 satellites in central Africa (McCollum et al., 2000; Yin and Gruber, 2010; Awange et al., 2016; Nicholson et al., 2018), it is
 not surprising that the GPCC-based products generally displayed higher errors.

Table 1: Root mean square errors (RMSEs) for the five P datasets (in three triplets) evaluated in this study, as well as the weighting factors used to unify the three most accurate datasets. All values are in units of cm/month.

Dataset	RMSE Triplet 1	RMSE Triplet 2	RMSE Triplet 3	Mean RMSE	Weighting Factor
TRMM 3B43	1.67	-	-	1.67	-
GPCC Version 7	-	1.66	-	1.66	-
PERSIANN-CDR	-	-	1.60	1.60	0.19
NIC131-gridded	0.65	0.72	0.60	0.65	0.47
CHIRPS2	0.93	0.88	0.96	0.93	0.33

265

TRMM, GPCC, and PERSIANN-CDR—which all integrate GPCC rain gauges in some capacity—are highly
 correlated and therefore feature similar RMSEs between 1.60 cm/month (PERSIANN-CDR) and 1.67 cm/month (TRMM).
 Therefore, our subsequent analyses discard GPCC and TRMM and use only PERSIANN-CDR—the most accurate of the three
 GPCC gauge-related datasets. As discussed in Sect. 2.2, PERSIANN-CDR was implemented in a weighted average in
 270 combination with NIC131-gridded and CHIRPS2 to create a unified P time series, P_{TC} . The NIC131-gridded only lasts through
 2014, so from 2015–2016 only CHIRPS2 and PERSIANN-CDR were used in P_{TC} . The uncertainty in P_{TC} was estimated to be
 0.30 cm/month from 2002–2014 and 0.59 cm/month from 2015–2016 (after NIC131-gridded data coverage ends)—both lower
 than the RMSEs of any of the individual P products tested.

3.2 Water balance ET estimates

275 In Fig. 1, clear seasonal cycles as well as interannual variations are visible in all four of the hydrologic fluxes from Eq. 1: the
 rainy MAM and SON seasons show local peaks in ET_{wb} as well as dS/dt , which is generally a negative flux (representing water
 leaving the land surface system) for most of the rest of the year. Q has the least temporal variability of the fluxes and is the
 smallest in magnitude, although it exhibits increased runoff 1–2 months after the primary SON rainy season. Mean annual
 ET_{wb} is 117.2 ± 3.5 cm/year (calculated from 2003–2015, the data-complete years of the study period). Mean annual P_{TC} from
 280 2003–2015 is 150.4 ± 2.6 cm/year, and mean annual Q is 33.7 cm/year. The dS/dt , which fluctuates between positive and
 negative values, ranges from -3.2 to 3.7 cm/month on average.

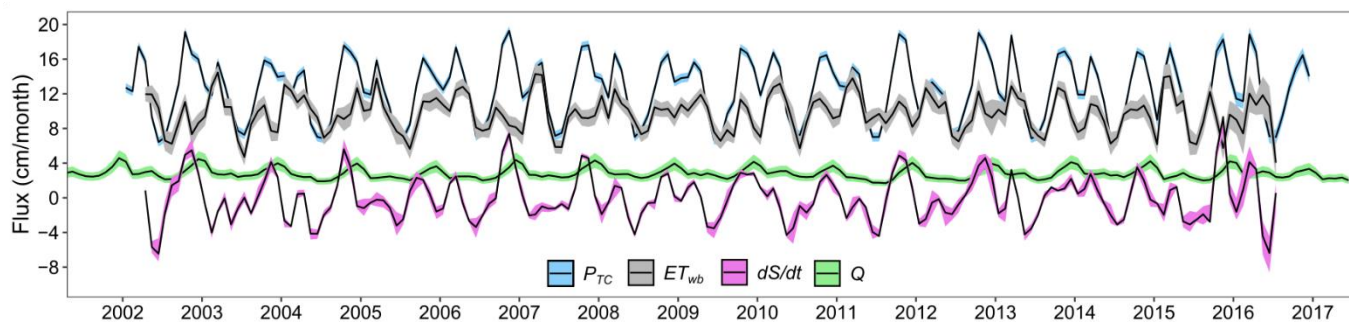
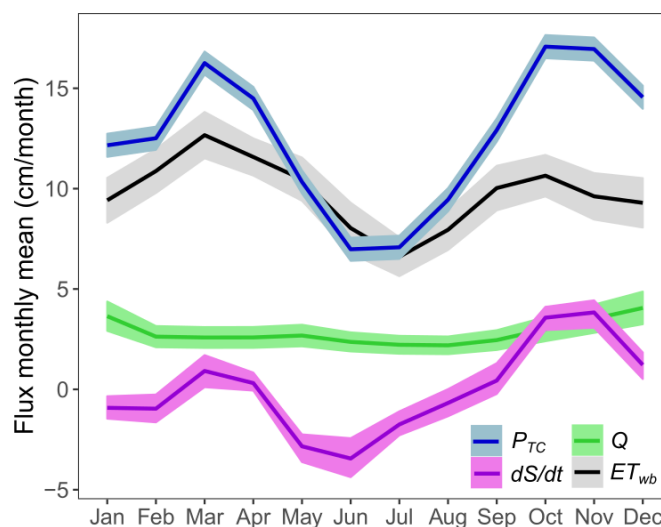


Figure 1: Time series of the four water balance components from 2002-2016. Data are monthly, basin-wide averages in cm water height equivalents. Black lines represent mean values; ribbons represent uncertainty ranges.

285 Plotting monthly means of the water balance fluxes provides further clarity regarding their seasonal cycles (Fig. 2).
 October and November are the rainiest months, followed by March and April, while June and July are the driest months of the
 year. The S regenerates mostly during the very wet October and November months and less so during December, the secondary
 rainy season in March and April, and in September with the onset of the primary rainy season. S loses water fastest during
 May and June, reaching its minimum during June, when ET_{wb} exceeds P_{TC} on average (Matsuyama et al., 1994). Interestingly,
 290 while ET_{wb} tracks the seasonality of P_{TC} to an extent, it peaks in March during the secondary rainy season rather than during
 the primary, wetter, SON wet season. The possible causes of this difference between precipitation and ET seasonality are
 analyzed further in Sect. 4.2.



295 **Figure 2: Mean monthly cycle of the four water balance components from 2002-2016. Dark lines represent mean values; ribbons represent uncertainties.**



Table 2 summarizes fourteen mean annual ET estimates from the Congo Basin found in the literature. The studies produce a mean ET of 116.7 cm/year with a standard deviation of 6.8 cm/year and a median ET of 118.9 cm/year, although different study periods and a variety of methods were used to estimate actual ET. All but one historical ET estimate fall within 10% of mean annual ET_{wb} , showing good agreement between the present study's ET estimates and prior literature on the subject.

Table 2: Historical estimates of mean annual basin-wide ET from the literature. Mean and median values are derived from the literature and presented alongside the mean annual ET_{wb} from this study.

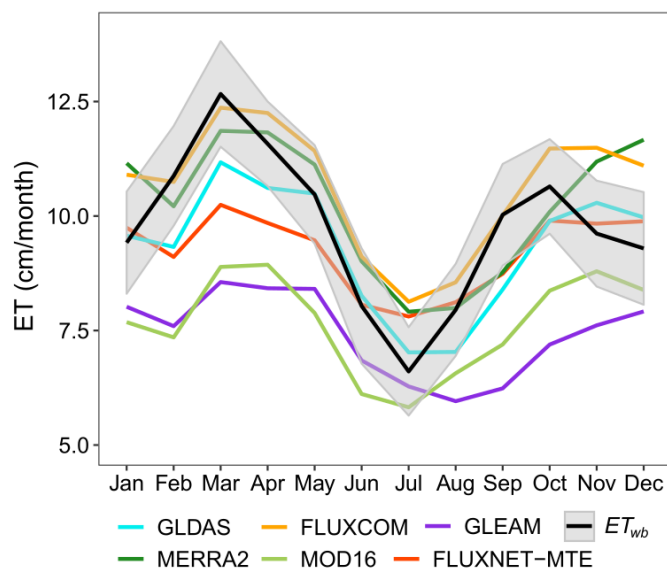
Source	Mean ET (cm/yr)	Time span
Balek 1977	124.8	climatology
Balek 1983	122.4	climatology
Bricquet 1988	123.0	climatology
Bultot 1971	119.6	climatology
Chishugi and Alemaw 2009	109.8	1961-1990
Matsuyama et al. 1994	125.0	1985-1988
Nicholson et al. 1997	112.7	climatology
Oki et al. 1993	120	1985-1988
Olivry et al. 1993	108.6	1951-1990
Pan et al. 2012	~102	1984-2006
Pinet and Souriau 1988	118.2	climatology
Russell and Miller 1990	114	climatology
Shem 2006	122.3	1979-1994
Ukkola and Prentice 2013	~111	1963-1998
Mean:	116.7	
Median:	118.9	
This study	117.2±3.5	2003-2015

3.3 Comparing the ET_{wb} seasonal cycle to global ET models

The seasonal cycle of ET_{wb} is compared to those of six global ET products in Fig. 3. Multiple datasets generally disagree with the magnitude of basin-wide ET_{wb} . Indeed, MOD16A2 and GLEAM v3.1a fall outside the uncertainty range of ET_{wb} more often than not. GLDAS-Noah and FLUXCOM monthly means both fall within the uncertainty range of ET_{wb} eight months out of the year, while MERRA2 does so seven months out of the year. While all models display the basin's low JJA ET to some degree, they generally fail to capture the fast recovery of ET_{wb} from August–September. Most models also correctly find ET to peak during the MAM rainy season (Matsuyama et al., 1994; Pan et al., 2012; Crowhurst et al., 2020), but all global ET products underestimate how much larger the MAM ET_{wb} peak is than the SON one. For instance, FLUXNET-MTE plots SON ET as roughly equivalent to MAM ET. The peak ET months for each rainy season also lag those of ET_{wb} for several products.



In general, the global ET products fail to capture the magnitude of seasonal variations in ET_{wb} , although some track ET_{wb} much more closely than others.



315 **Figure 3: Mean monthly cycle of ET_{wb} plotted alongside the mean monthly cycles of six global ET products. The grey ribbon represents ET_{wb} uncertainty.**

Global ET products are evaluated against ET_{wb} from 2003–2011 using several metrics in Table 3. Mean annual ET ranges from 88.7 cm/year (GLEAM v3.1a) to 127.6 cm/year (FLUXCOM), compared to the ET_{wb} annual mean of 118.0 ± 3.5 cm/year for that time period. Excepting GLEAM v3.1a and MOD16A2, the global ET product annual averages all fall within
320 10% of ET_{wb} 's. FLUXCOM produces the highest Pearson correlation coefficient versus ET_{wb} while MERRA2 produces the lowest, and FLUXCOM again leads all products in Taylor skill score while FLUXNET-MTE demonstrates the lowest. FLUXCOM also features the lowest RMSE relative to ET_{wb} ; GLEAM v3.1a features the highest. GLEAM v3.1a underestimates mean annual ET_{wb} by nearly 25%, exhibits a low Taylor score, and has the highest RMSE of all six products. MOD16A2 has the second-highest RMSE of the six products evaluated and generally underestimates the magnitude and
325 seasonality of ET_{wb} in the Congo Basin while achieving a correlation coefficient of only 0.54 and a Taylor score of 0.58.



Table 3: Mean annual ETs from 2003-2011 alongside Pearson correlation coefficients, Taylor skill scores, RMSEs, and standard deviations from 2002-2011 for six global ET products in comparison to ET_{wb} .

ET product	Mean annual ET (cm)	Pearson correlation coefficient	Taylor skill score	RMSE (cm)	Standard Deviation
ET_{wb}	118.0±3.5				2.1
MOD16A2	94.2	0.54	0.58	2.7	1.3
GLEAM	88.7	0.53	0.40	3.0	0.9
FLUXNET-MTE	111.1	0.63	0.36	1.8	0.8
FLUXCOM	127.6	0.74	0.71	1.6	1.3
GLDAS-Noah	110.7	0.64	0.69	1.7	1.4
MERRA2	119.7	0.43	0.68	2.1	1.7

3.4 Drivers of ET seasonality and variability

As discussed in Sec 3.2, the shape of ET_{wb} 's seasonal cycle roughly follows that of P_{TC} , since water availability and vegetation productivity modulate ET. However, ET_{wb} is greater during the MAM rainy season than in the SON rainy season, despite the latter being wetter than the former. On average, ET_{wb} also exceeds P_{TC} during June. These findings are consistent with previous studies that found basin-wide ET can peak during MAM (Matsuyama et al., 1994; Pan et al., 2012; Crowhurst et al., 2020), although the drivers behind this seasonal cycle are less clear. To help develop hypotheses on the nature of ET's drivers, monthly mean ET_{wb} is compared to several climatic drivers and indices reflecting seasonally varying vegetation activity (Fig. 4).

Possible environmental drivers of the ET_{wb} seasonality include soil water availability, water demand from VPD, radiation, and temperature. GRACE-derived S can be assumed to be a partial proxy for water availability (though note that not all water measured by S is necessarily accessible to plant roots or available for soil evaporation; see Sect. 4.2.4). S is significantly lower during SON than MAM (Fig. 4f), consistent with the relatively lower SON ET_{wb} . The relatively lower SON S could be due to the much lower precipitation during JJA than DJF (Fig. 3) and/or due to a difference in how much of the rainfall infiltrates the land surface. VPD is fairly low in both wet seasons, although still elevated in September following the JJA dry season (Fig. 4e). R_n is lower during the SON wet season than the MAM, likely contributing to the lower ET_{wb} in SON.

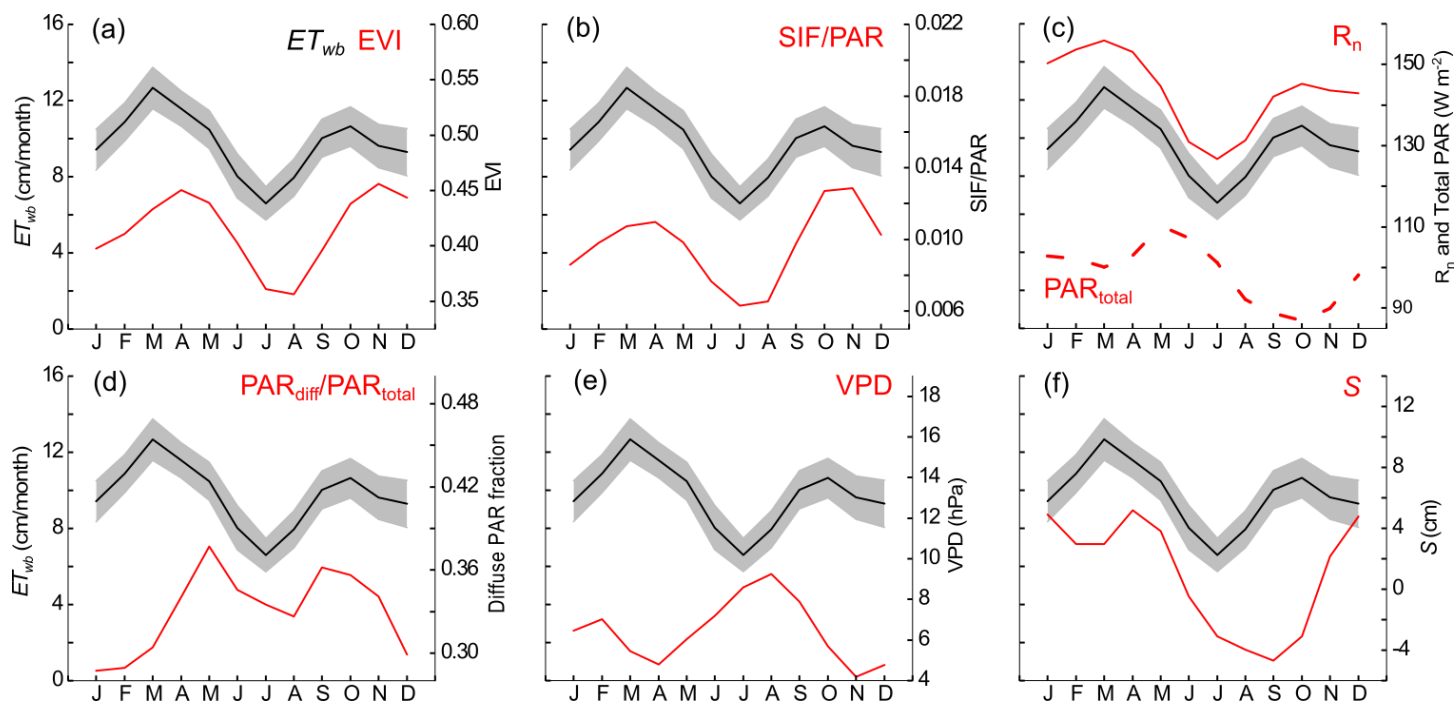


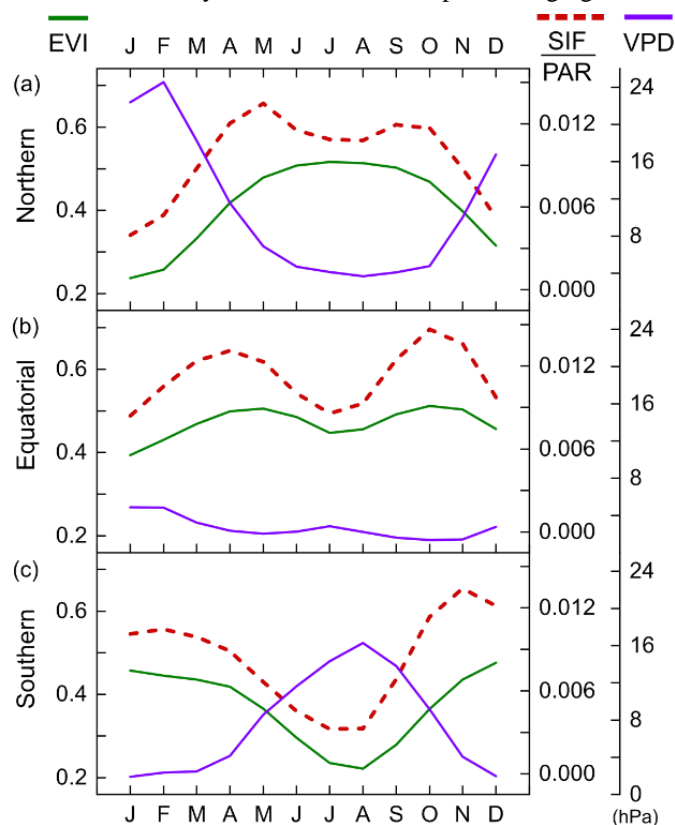
Figure 4: Mean monthly cycle of ET_{wb} (black line with gray uncertainty range) plotted alongside those of (a) MAIAC-processed EVI, (b) SIF/PAR, (c) R_n and total PAR, (d) Diffuse PAR fraction (PAR_{diff}/PAR_{total}), (e) VPD, and (f) S from GRACE (red lines). Data are averaged over the entire basin area. Note that the mean ET_{wb} curve and scale is the same in each sub-panel.

The variability of ET is expected to be linked to vegetation phenology through the large contribution of transpiration to overall ET in the densely vegetated Congo Basin (Lian et al., 2018). However, both MAIAC EVI (Fig. 4a) and PAR-normalized SIF (Fig. 4b) show greater vegetation greenness and photosynthesis, respectively, during the SON wet season than during the MAM wet season. This suggests relatively greater water use efficiency (WUE) in SON and/or a relatively greater contribution of direct soil/canopy evaporation to ET in MAM (although bare soil evaporation is expected to be a minority of total ET in the densely-forested basin; see Sect. 4.2). This greater water use efficiency during the SON than the MAM season could also be driven by a relatively greater ratio of diffuse PAR to total PAR during SON (Fig. 4d) which can increase photosynthetic efficiency (Mercado et al., 2009), as further discussed in Sect. 4.2.3.

The basin-wide analyses in Fig. 4 are almost certainly masking significant sub-basin variability. The sub-basin division of ET is not known, and dividing the coarse-resolution S at the sub-basin level is also highly uncertain. Nevertheless, we considered the sub-basin variation of select productivity and climatic metrics (Fig. 5). The basin was divided into the equatorial evergreen forest (which straddles the equator), Northern deciduous ecosystems, and Southern deciduous ecosystems (Fig. S2). The deciduous regions feature larger seasonal variations in all three variables than the evergreen forest (Fig. 5), but the opposite seasonalities of the Northern and Southern regions partially offset one another and produce basin-wide EVI and SIF/PAR cycles that are broadly similar to those of the evergreen forest (Figs. 4a, b; 5b). The greater extent of the Southern



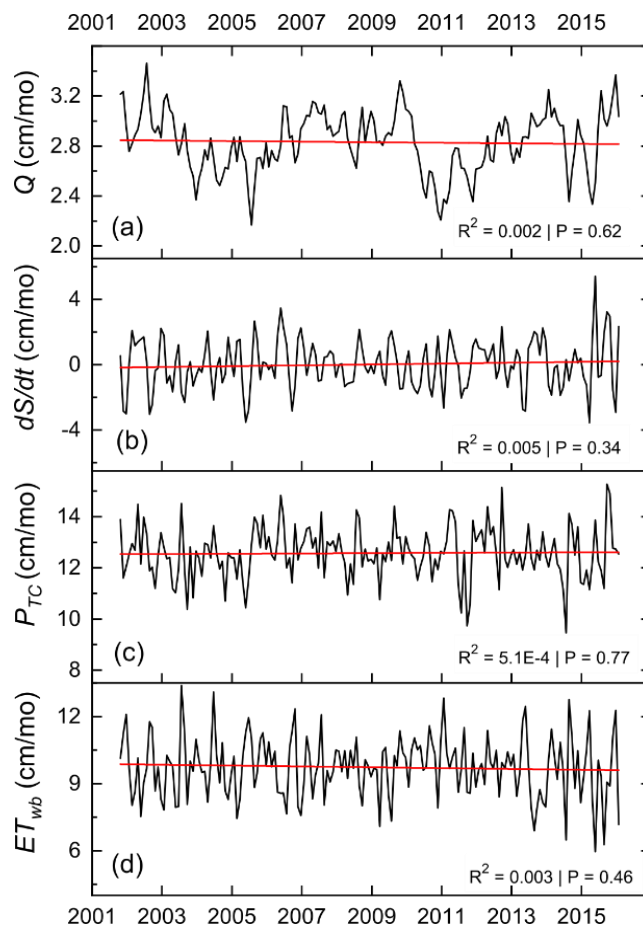
deciduous region results in basin-wide EVI and SIF/PAR minima during JJA rather than DJF, and basin-averaged VPD likewise peaks during JJA (Fig. 5e) despite its low variability in the extensive evergreen forest region (Fig. 5b). Taken together, the results of Fig. 5 suggest that a basin-wide analysis is informative despite averaging over multiple vegetation types.



365 **Figure 5:** (a) Average monthly cycles of MAIAC-processed EVI (green line), SIF/PAR (red dashed line), and VPD (purple line) for the northern deciduous area of the Congo Basin. (b)-(c) As with (a), but for the equatorial evergreen and southern deciduous regions, respectively. Scales are consistent between plots (a)-(c) for each variable.

3.5 Long-term climatic shifts and their impacts in the Congo Basin

We detect no significant linear trends in ET_{wb} , P_{TC} , dS/dt , or Q from 2002–2016 after removing average seasonal cycles with BFAST (Fig. 6). However, several interannual trends are detectable in other environmental data (Fig. 7). PAR, R_n , and VPD
 370 all increase significantly from 2002–2016 after the average seasonal cycle is removed from the time series, indicating the Congo Basin has become sunnier and less humid in recent years. This progression to sunnier and less humid conditions in the Congo Basin is not reflected in ET_{wb} and productivity (as measured by MAIAC EVI), which do not show long-term changes over the past two decades (Figs. 6d, 7d).



375 **Figure 6: Linear regressions of deseasonalized monthly (a) Q , (b) dS/dt , (c) P_{TC} , and (d) ET_{wb} .**

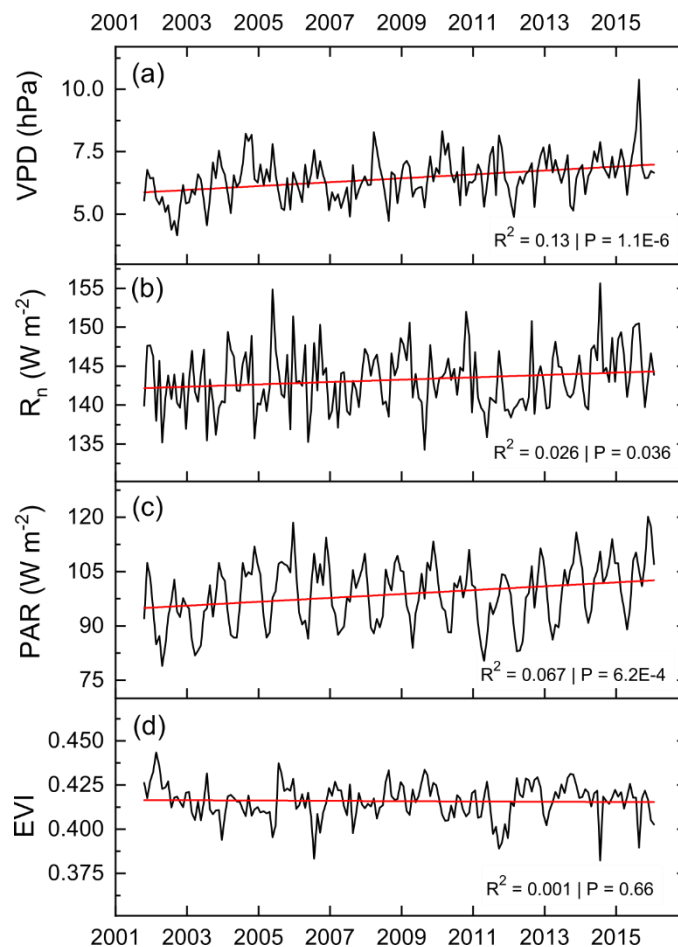


Figure 7: Linear regressions of deseasonalized monthly (a) VPD, (b) R_n , (c) PAR_{total} , and (d) MAIAC EVI.

4 Discussion

4.1 The value of water balance-based ET estimation in the Congo Basin

380 The scarcity of operational precipitation gauges and complete lack of eddy covariance towers within the Congo river basin
have previously restricted ET estimates to process-based models, short-term ET observations at site scale, and global products
with insufficient validation in tropical Africa. The water balance-based ET_{wb} derived here provides a basin-wide constraint on
ET. It has an uncertainty that is relatively low compared to its average seasonal cycle (Fig. 2), and its magnitude matches well
with previous long-term ET estimates from the basin (Table 2). The shape of its annual seasonal cycle (with ET_{wb} peaking in
385 MAM rather than in SON) also agrees with several previous ET modeling efforts in the basin (Matsuyama et al., 1994; Pan et
al., 2012; Crowhurst et al., 2020). These findings support the accuracy of the water balance model in estimating basin-wide



ET, and indicate the combination of P products used is relatively accurate when considered across the basin and aggregated using triple collocation.

4.2 The seasonal imbalance of ET_{wb} and P maxima

390 As expected, the seasonal cycle of ET_{wb} mostly follows that of precipitation, with two annual dry and two annual wet seasons. However, the seasonal cycles of P and ET_{wb} feature an interesting offset: whereas SON is the wetter of the two rainy seasons, ET_{wb} is greater during MAM than during SON (Fig. 2). The ET_{wb} peak during MAM is supported by several previous modeling efforts with a variety of methodologies (Matsuyama et al., 1994; Pan et al., 2012; Crowhurst et al., 2020), indicating it is not simply an artifact of the water balance model or the data sources used here. Yet the underlying causes of the imbalance are not well understood (Crowhurst et al., 2020). We evaluated several possible drivers of the observed MAM peak in ET_{wb} including phenology, photosynthetic production (via EVI and SIF), terrestrial water availability (via GRACE-derived S), PAR, R_n , VPD, T_a , and T_s . Ultimately, we conclude that the availability of radiative energy (especially photosynthetically-favorable diffuse radiation) and greater soil water availability during MAM provides the most likely explanation for its high ET rates.

As transpiration is the dominant component of ET throughout the Congo Basin (Lian et al., 2018), primary productivity (through its links to stomatal closure and active leaf area) likely explains the seasonality of ET_{wb} to some degree. In fact, recent studies have found that evergreen forests in equatorial Africa exhibit a similar greenness seasonality to the seasonality of ET_{wb} , with a bimodal cycle generally aligning with P but peaking in MAM instead of the wetter SON (Betbeder et al., 2014; Philippon et al., 2016). However, these studies used MODIS products that did not fully account for sun-sensor geometry and other sources of error at low latitudes. To this end, the MAIAC algorithm (Lyapustin et al., 2012) reduces noise and increases the availability of clear-sky data in wet tropical regions (Maeda et al., 2016). Here, we found that after correction with the MAIAC algorithm, EVI data from the evergreen forest region do not present any significant difference between the two rainy seasons (Fig. 5b), and basin-wide MAIAC EVI appears to peak during SON rather than MAM (Fig. 4a). Furthermore, direct estimation of photosynthetic rates using SIF/PAR data reveals greater productivity in SON than MAM throughout the evergreen forest band (Fig. 5b) and the basin as a whole (Fig. 4b). The misaligned seasonal peaks of SIF/PAR and ET_{wb} indicate that either a) water use efficiency (WUE) varies seasonally when generalized across the basin, resulting in higher MAM transpiration but lower MAM photosynthesis, or b) that the MAM peak in ET is primarily driven by direct evaporation from the canopy or land surface rather than transpiration.

4.2.1 Leaf age-related WUE variations

Leaf age offers a possible explanation for the variable WUE hypothesis. Studies of tropical trees have found that new leaves can take 1–2 months to reach peak photosynthetic capacity and WUE, and that both traits tend to decline as leaves reach 5–6 months old (Sobrado, 1994; Shirke, 2001). Leaf age has been linked to photosynthetic seasonality within the Amazon rainforest (Wu et al., 2016), although this effect has not been investigated in the Congo basin. Connecting the phenology of Congolese forests to basin-wide photosynthesis and transpiration must account for multiple broad ecoregions that span the



equator and therefore face inverted seasonalities (Figs. 5, S2). In much of the deciduous woodlands of the northern (southern)
420 basin, vegetation leaf flushing tends to begin 1–2 months prior to the onset of MAM (SON) rains and senescence begins around
the end of the SON (MAM) rains, but both processes occur over the course of 1–2 months (Guan et al., 2014; Vinya et al.,
2019). Likewise, microwave backscatter data from large areas of the Congo’s evergreen forest imply dry season leaf flushing
likely occurs during DJF and JJA (Guan et al., 2013; Konings et al., 2017). Note, however, that phenological synchronicity
appears to be low in the evergreen forests of central Africa (Couralet et al., 2013), so the magnitude and effects of evergreen
425 leaf flushing are probably smaller and more temporally distributed in the evergreen forests than in the deciduous woodlands
of the basin.

After accounting for the different ecoregions within the Congo Basin, leaf age effects alone appear unable to explain
the flipped seasonality of ET_{wb} in the two rainy seasons: although WUE increases as leaves mature, overall transpiration rates
in tropical deciduous leaves remain high until they reach old age (Sobrado, 1994; Shirke, 2001). Thus, July–August leaf
430 flushing of the southern deciduous woodlands, which far exceed the northern woodlands in area (Fig. S2), would most likely
increase basin-wide transpiration alongside photosynthesis during SON. While our current understanding of regional
phenology appears broadly consistent with remotely-sensed vegetation data, better field observations of phenology, leaf age,
and associated changes in stomatal conductance and productivity in the different ecosystems of the Congo basin are needed to
fully determine the role of vegetation in modulating ET seasonality.

435 4.2.2 VPD and temperature

Climatic conditions beyond precipitation could also contribute to the seasonal variations in WUE. For instance, high
VPD reduces WUE by drawing more water from stomata per unit of carbon intake during transpiration. Basin-averaged VPD
data from the ERA-Interim reanalysis do not indicate that MAM conditions are significantly less humid than SON conditions
(Fig. 4e), suggesting seasonal VPD variations cannot explain the flipped ET_{wb} –precipitation wet season magnitudes. But the
440 uncertainties in reanalysis-based temperature and humidity data from tropical regions (Lorenz and Kunstmann, 2012; Brands
et al., 2013) warrant an examination of the limited in-situ data available from within the Congo Basin. Observational VPD
data from weather reports show that while ERA-Interim captures the shapes of seasonal VPD cycles fairly accurately, it fails
to capture the magnitude of daytime VPDs in the evergreen rainforest (Fig. S1). Further examination of station and reanalysis
data from within the evergreen forest region shows that rainforest VPD is slightly greater during MAM than SON (Figs. 5b,
445 S1c–f), consistent with models based on historical pan evaporation data across the basin (Bultot, 1971) and historical
atmospheric humidity data from within the equatorial rainforest (Lauer, 1989). However, because evergreen rainforest VPDs
are generally low compared to other regions of the basin (Fig. 5) and are only slightly greater during MAM (Fig. S1c–f), VPD
is not expected to be a significant driver of ET variations at basin-wide scales.

While basin-averaged T_a does not vary drastically throughout the year, T_s features a bimodal seasonality that peaks
450 primarily in September and also from February to March (Fig. S3). T_s can regulate ET via stomatal conductance, which tends
to increase with leaf temperature to a point, although a wide range of sometimes-contradictory results have been published on



455 this matter (Urban et al., 2017). In this case, the poor alignment of peak T_s and ET_{wb} values—taken in conjunction with the widespread stomatal closures known to occur in tropical forests during the hottest parts of the day (Fisher et al., 2006; Konings and Gentine, 2017; Konings et al., 2017)—indicate that other variables are more directly responsible for the high ET_{wb} observed during MAM.

4.2.3 Radiative fluxes

The magnitude and quality of radiative fluxes can drive the dynamics of ET_{wb} by influencing primary production as well as WUE. R_n and total PAR are both diminished in SON relative to MAM levels (Fig. 4c), which does not explain the SON peak in primary production observed in SIF/PAR and EVI data (Fig. 4a, b). However, greater R_n levels during MAM
460 could decrease WUE by increasing water demand, thereby driving the high ET_{wb} levels observed in MAM.

Additionally, the quality of PAR beyond the flux's magnitude could affect WUE and explain the apparent decoupling of productivity from irradiance levels and ET_{wb} . Prior studies have found that increasing PAR_{diff}/PAR can increase WUE and light use efficiency (LUE) in tropical savannahs and global forest canopies, including in an Amazonian tropical broadleaf stand (Alton et al., 2007; Kanniah et al., 2013). Furthermore, total canopy ET has been found to decrease as the diffuse light fraction
465 increases (Rocha et al., 2004). Philippon et al. (2019) examine diffuse and direct irradiance data from the Breathing Earth System Simulator (BESS; Ryu et al., 2018) and the Satellite Application Facility for Climate Monitoring (CM-SAF; Müller et al., 2015) and find that the ratio of direct irradiance is often higher during MAM than in SON throughout much of the Congo Basin. The CERES data produce similar results: while PAR_{diff}/PAR peaks in May, on average it is significantly lower during the MAM season than during SON. PAR_{diff}/PAR remains low throughout March (the month when ET_{wb} peaks) and the greater
470 total PAR flux in MAM is mostly attributable to greater PAR_{dir} (Fig. S4). After removing seasonal cycles and long-term trends, monthly mean SIF/PAR displays a strong negative correlation with mean PAR_{dir} but not with PAR_{diff} , indicating photosynthetic rates do not scale as well with increasing direct sunlight as with diffuse sunlight (Fig. S5). These experiments suggest the quality of insolation during SON could allow for higher photosynthetic rates with lower ET than during MAM, especially since monthly PAR_{diff}/PAR in the Congo remains below 0.4 on average (Kanniah et al., 2013) and lower R_n corresponds to
475 lower water demand (Philippon et al., 2019). Even if total PAR availability would favor a productivity peak in MAM, lower WUE and LUE could result in plants transpiring all available water without reaching the productivity levels achieved in SON. Thus insolation quality potentially explains ET_{wb} 's imbalanced seasonality.

4.2.4 Terrestrial water storage

The availability of water in the rooting zone can modulate ET_{wb} by directly limiting transpiration during SON. Even
480 though P during MAM is significant, dS/dt (which measures groundwater within the rooting zone as well as in deeper reserves) remains much lower than its SON levels and only seems to recharge S enough to compensate for the slightly negative dS/dt values of January and February (Fig. 2), indicating that water reserves are largely saturated during MAM and undersaturated at the onset of SON (Fig. 4f). This hypothesis is consistent with prior soil moisture modeling efforts, which indicate that



Congolese ecosystems south of the equator (i.e. most of the basin's area) feature low soil moisture as SON rains begin before
485 maintaining high soil moisture and deeper water reserves through the end of the MAM rainy season (Pokam et al., 2012; Guan
et al., 2014). Terrestrial water reserves are well-known to modulate productivity/ET throughout the basin (Saeed et al., 2013;
Guan et al., 2014; Ndehedehe et al., 2018; Cuthbert et al., 2019), so depleted S during September and October could limit
transpiration even after the dry season ends. This hypothesis is also consistent with recent findings that variability in soil
moisture and groundwater are much more influential than variability in rainfall with regard to productivity anomalies within
490 the Congo Basin (Madani et al., 2020), making variations in plant-available soil moisture a plausible driver of the seasonal
 ET_{wb} imbalance when combined with the light quality impacts on WUE outlined in the previous section.

4.2.5 Direct canopy and soil evaporation

The WUE hypotheses explored above largely focus on the seasonality of transpiration, but seasonal variability in
direct evaporation from forest canopies and the soil system could also potentially influence the seasonal cycle of ET_{wb} . As
495 outlined above, R_n is lower in SON than during MAM (Fig. 4c), suggesting that there may simply be less energy driving direct
evaporation of water from the land surface. As R_n and ET_{wb} both peak in March and high water content in the soil surface layer
is apparently sustained throughout the rainy seasons (Guan et al., 2014), the conditions seem appropriate to drive increased
direct evaporation during MAM. However, the higher proportion of nighttime rains during these months (Philippon et al.,
2016) make this scenario less plausible, as recent rainfall would have more time to drip from the canopy to the soil surface and
500 percolate to deeper soil levels. Additionally, a recent study of several climate models within the Congo Basin determined that
soil and canopy evaporation rates are likely similar between the two wet seasons, and that the ET_{wb} seasonal imbalance is more
likely due to increased transpiration during MAM (Crowhurst et al., 2020). More research is required to definitively
characterize the role of direct evaporation in the seasonality of ET, but given the dominance of transpiration as the primary
component of ET within the Congo Basin (Lian et al., 2018) and the conclusions of Crowhurst et al. (2020), we find it unlikely
505 to be the main driver of ET_{wb} 's MAM peak.

Taken together, the analyses above suggest that the timing of peak ET rates in MAM rather than SON is primarily
due to a combination of greater moisture availability and higher R_n during MAM, as well as the higher fraction of diffuse
radiation during that season. The decoupled seasonal peaks of ET_{wb} and photosynthetic productivity also indicate that seasonal
variations in WUE occur across the Congo Basin.

510 4.3 Comparison to global ET products

The six global ET models evaluated generally do not capture the amplitudes of interannual and seasonal variability displayed
by ET_{wb} (Fig. 3, Table 3). Broadly speaking, FLUXCOM and to a lesser degree GLDAS-Noah appear to lead global ET
products in reproducing ET_{wb} . However, both of these products have significantly lower temporal standard deviations than
 ET_{wb} does. Indeed, all alternative ET products have less temporal variability than ET_{wb} , ranging from only ~40% of the ET_{wb}
515 variability (FLUXNET-MTE) to at most 80% of it (MERRA-2). These metrics reflect the fact that global ET models tend to



repeat the same seasonal ET cycle every year with only minor interannual variability. Although some products feature relatively accurate seasonal cycles (Fig. 3), ET_{wb} features significant departures from its mean season cycle in any given year (Fig. 1) that are not reflected in the six ET products evaluated here.

Our results show some disagreements with the previous model comparison efforts of Liu et al. (2016). As part of a
520 global water balance-based assessment of ET products, Liu et al. (2016) also compare ET_{wb} (estimated using a different
approach; see below) to ET from GLEAM, FLUXNET-MTE, GLDAS-NOAH Version 2, and MERRA in the Congo Basin.
However, in our calculation, the Taylor skill score of GLDAS-2.1 appears to far outperform its value in Liu et al. (2016),
FLUXNET-MTE and MERRA2 both show modest improvements in their Taylor scores, and GLEAM v3.1a falls slightly short
of its previous value. These discrepancies were likely caused by a) the different study period used by Liu et al. (2016), which
525 necessitated an extrapolation of GRACE data prior to 2002, b) the exclusive use of the GPCC Version 6 product to constrain
 P in their water balance models, and c) the use of different versions of the four datasets common to both Liu et al. (2016) and
the present study. Nonetheless, comparison of these Taylor scores indicates that the most recent generation of ET products
generally improved upon the previous generation (GLEAM being the only partial exception): FLUXCOM outperforms its
predecessor, FLUXNET-MTE; GLDAS-NOAH Version 2.1 outperforms Version 2.0; and MERRA Version 2 improves upon
530 MERRA Version 1's skill score.

Out of the six comparison products, the two remote sensing-based products diverge the most from ET_{wb} , despite being
the most observationally-driven. While some previous studies have found MODIS-derived ET to approximate actual ET fairly
well in nearby regions in West Africa (Schüttemeyer et al., 2007; Opoku-Duah et al., 2008; Andam-Akorful et al., 2015), the
results of this comparison reinforce the value of ET_{wb} as a data-driven, independent estimate of a critical hydrological flux.

535 4.4 Effects of long-term climatic shifts on ET

From 2002–2016, no significant trend is detectable in the deseasonalized ET_{wb} data, nor in any of the other water balance
component fluxes (Fig. 6). The lack of significant trends in water balance components over the fifteen-year study period is
surprising given the numerous reports of declining precipitation in the Congo Basin, both in magnitude (Asefi-Najafabady and
Saatchi, 2013; Diem et al., 2014; Zhou et al., 2014; Hua et al., 2016; Dezfuli, 2017) and seasonality (Jiang et al., 2019).
540 However, the absence of a trend in P_{TC} does not indicate the absence of a longer-term drying trend that began in the 20th
century—rather, it probably results from our study period, which is shorter and generally more recent than those of the
aforementioned studies, and our analysis of rainfall over all seasons rather than during certain three-month windows. Indeed,
careful examination of long-term precipitation plots reveals marked declines in rainfall during the 1990s and early 2000s that
did not continue significantly into our 2002–2016 study period (Diem et al., 2014; Dezfuli, 2017; Hua et al., 2019). The lack
545 of an interannual ET_{wb} trend is consistent with the recent findings of Weerasinghe et al. (2020).

The lack of long-term trends in ET_{wb} and EVI is nevertheless surprising given the changes detectable in the other
environmental variables (Figs. 7, S6): PAR_{diff} , PAR_{dir} , R_n , and VPD all increase significantly from 2002–2016, indicating the
Congo Basin has become sunnier and less humid in recent years. While meteorological data are quite sparse in the basin during



550 this fifteen-year period, the increasing VPD trends in ERA-Interim are consistent with projections of rising VPD in CMIP5 models (Yuan et al., 2019). Sunnier and less humid conditions would typically lead to lower WUE in plants, which would in turn lead to increased ET and/or decreased EVI. Given the seasonal dependence of productivity and transpiration on irradiance levels (see Sect. 4.2.3), the apparent lack of a corresponding long-term relationship indicates that some mechanism may be counteracting the biological impacts of rising irradiance and VPD.

555 Carbon fertilization offers one possible explanation for the lack of ET_{wb} and EVI trends. Rising VPD can indeed reduce the WUE of vegetation, but conversely, rising atmospheric CO_2 levels can increase WUE in tropical forests by catalyzing stomatal closure (De Kauwe et al., 2013; Keenan et al., 2013; Van Der Sleen et al., 2015). Ukkola and Prentice (2013)'s vegetation dynamics simulations yield a sizeable decrease in stomatal conductance between 1960 and 2000 in the Congo Basin, consistent with altered stomatal behavior from CO_2 fertilization and increasing VPD. Increasing PAR levels also could have helped support forest productivity rates as stomatal conductance declined, but the PAR data in Fig. S6 suggest a 560 continual decrease in diffuse PAR fraction that could adversely affect the WUE and LUE of Congolese forests (Kanniah et al., 2013). In summary, even as VPD and irradiance have increased and driven up evaporative demand in plant stomata, the rising concentration of atmospheric CO_2 has seemingly allowed the Congo's forests to lower stomatal conductance without significantly impacting growth or ET (Peñuelas et al., 2011; Van Der Sleen et al., 2015). But the effects of present and future carbon fertilization on WUE remain highly uncertain (Guerrieri et al., 2019). Thus, although ET did not show any statistically- 565 significant trends during our 2002–2015 study period, future ET rates could nevertheless start declining if the compensation between decreasing radiation quality and rising VPD on the one hand and increasing CO_2 on the other hand becomes imbalanced, or if long-term declines in precipitation continue.

5 Conclusions

570 This study leverages several remotely-sensed and gauge-based precipitation datasets, river gauge data, and terrestrial water storage anomalies from GRACE to produce ET estimates for the Congo Basin in central Africa. This technique has been successfully applied to the Amazon Basin in recent years, but to the authors' knowledge it has not yet been used in the Congo Basin except as part of global-scale reviews of major river basin. The Congo Basin is greatly understudied despite its importance as one of the world's largest river basins and one of three major humid tropical forest regions, and quantification of basin-wide ET and its variability is imperative for understanding the basin's influence on regional and global climates as 575 well as its susceptibility to environmental disturbances. We find annual ET_{wb} to equal 117.2 ± 3.5 cm/year, on average, from 2003–2015—well in line with many historical estimates of basin-wide ET.

580 Triple collocation was applied to determine the accuracy of P products over the sparsely-gauged Congo Basin, finding that the recently-developed NIC131-gridded dataset is the most accurate over our study period (RMSE of 0.65 cm/month). NIC131-gridded is followed by CHIRPS2 in terms of accuracy (RMSE of 0.93 cm/month), while three separate products that incorporate GPCC rain gauge data feature similar variability and RMSEs (1.60 to 1.67 cm/month). RMSEs from TC were also



used to create a unified P_{TC} time series with a mean annual precipitation of 150.4 ± 2.6 cm/year. A suite of global ET products is also evaluated versus ET_{wb} , with FLUXCOM and GLDAS-Noah Version 2.1 displaying the closest agreement with ET_{wb} from 2002–2011. However, all ET models underestimated the seasonal and interannual variability of ET_{wb} .

In good agreement with existing literature, rainfall appears to exert a primary control on ET, but other environmental drivers appear to modulate ET and cause unexpected seasonal features, such as the MAM peak in ET recently explored by Crowhurst et al. (2020). Several possible causes for this MAM ET peak were investigated, but neither VPD, temperature, phenology, or leaf age seasonalities could explain this MAM peak. Instead, the amount and quality of radiative energy and the availability of water in the terrestrial system appear to offer the most plausible explanation for the seasonal imbalance in peak ET_{wb} —higher diffuse PAR fractions and lower R_n during SON allow for higher WUE, while depleted terrestrial water stores limit the amount of water available for transpiration. On interannual timescales, VPD, R_n , and both direct and diffuse PAR increased from 2002–2016 while no trend was detectable in EVI and ET_{wb} , implying the rising concentration of atmospheric CO_2 has compensated for the increasingly dry conditions facing the Congo Basin's forests. However, these effects may not remain balanced in a future of higher CO_2 levels, increased VPD and temperatures, and spreading deforestation within the basin.

595 **Author contributions**

AGK and MWB designed the study. MWB and GRQ retrieved the data. All authors analyzed the data. MWB prepared the manuscript with the assistance of AGK and GRQ.

Data availability

We provide our monthly basin-wide P , ET_{wb} , dS/dt , discharge, and other data online at
600 <http://doi.org/10.17605/OSF.IO/JPVMB>.

Most of the original data products used in this study are freely available to the public: the HydroSHEDS basin boundary shapefile can be retrieved from <https://hydrosheds.org/page/hydrobasins>. PERSIANN-CDR data were accessed at <http://dx.doi.org/10.7289/V51V5BWQ> and CHIRPS2 data were downloaded from <https://www.chc.ucsb.edu/data>. The GPCC dataset was accessed at <https://www.esrl.noaa.gov/psd/>. GRACE data were retrieved from GRCTellus Land at <http://grace.jpl.nasa.gov>, and Congo River discharge data were downloaded from HYBAM at <http://www.ore-hybam.org>. FLUXNET-MTE and FLUXCOM were made available by the Max Planck Institute for Biogeochemistry; FLUXCOM may be accessed at <http://fluxcom.org>. GLEAM data were accessed at <http://gleam.eu>. TRMM, MERRA-2, and GLDAS-Noah data were provided by NASA GES DISC at <https://disc.gsfc.nasa.gov/>. CERES data were downloaded from
610 https://ceres.larc.nasa.gov/order_data.php. ERA-Interim data were retrieved from the ECMWF at



<https://www.ecmwf.int/en/forecasts/datasets>, MOD16A2 and MCD12C1 data were downloaded from the USGS website at <https://lpdaac.usgs.gov/products/mod16a2v006/> and <https://lpdaac.usgs.gov/products/mcd12c1v006/>, respectively, and AIRS data were downloaded from NASA's Giovanni web interface (<https://giovanni.gsfc.nasa.gov/giovanni/>). ASOS and MIDAS weather data were sourced from the UK Met Office's CEDA website at <http://catalogue.ceda.ac.uk/uuid/220a65615218d5c9cc9e4785a3234bd0> and from Iowa State University's Iowa Environmental Mesonet site at <https://mesonet.agron.iastate.edu/ASOS/>.

Competing interests

The authors declare that they have no conflict of interest.

Acknowledgements

We gratefully acknowledge the researchers who provided their datasets and expertise for this study: A. Lyapustin and Y. Wang of NASA provided the MAIAC EVI data; S. Nicholson and D. Klotter of Florida State University provided their NIC131-gridded dataset; and J. Joiner of NASA provided the GOME-2 SIF data. C. Frankenberg of the California Institute of Technology graciously provided additional SIF data for comparison. MWB was supported by a Stanford University Vice Provost for Undergraduate Education (VPUE) grant. This work was also supported by NASA Terrestrial Ecology award 80NSSC18K0715 through the New Investigator Program, by the NASA Carbon Cycle Science program, and by NOAA grant NA17OAR4310127.

References

- Alemohammad, S. H., McColl, K. A., Konings, A. G., Entekhabi, D. and Stoffelen, A.: Characterization of precipitation product errors across the United States using multiplicative triple collocation, *Hydrol. Earth Syst. Sci.*, 19, 3489–3503, <https://doi.org/10.5194/hess-19-3489-2015>, 2015.
- Alemohammad, S. H., Fang, B., Konings, A. G., Aires, F., Green, J. K., Kolassa, J., Miralles, D., Prigent, C. and Gentine, P.: Water, Energy, and Carbon with Artificial Neural Networks (WECANN): a statistically based estimate of global surface turbulent fluxes and gross primary productivity using solar-induced fluorescence, *Biogeosciences*, 14, 4101–4124, <https://doi.org/10.5194/bg-14-4101-2017>, 2017.
- Alsdorf, D., Beighley, E., Laraque, A., Lee, H., Tshimanga, R., O'Loughlin, F., Mahé, G., Dinga, B., Moukandi, G. and Spencer, R. G. M.: Opportunities for hydrologic research in the Congo Basin, *Rev. Geophys.*, 54, 378–409, <https://doi.org/10.1002/2016RG000517>, 2016.
- Alton, P. B., North, P. R. and Los, S. O.: The impact of diffuse sunlight on canopy light-use efficiency, gross photosynthetic



- product and net ecosystem exchange in three forest biomes, *Glob. Chang. Biol.*, 13, 776–787, <https://doi.org/10.1111/j.1365-2486.2007.01316.x>, 2007.
- 640 Andam-Akorful, S. A., Ferreira, V. G., Awange, J. L., Forootan, E. and He, X. F.: Multi-model and multi-sensor estimations of evapotranspiration over the Volta Basin, West Africa, *Int. J. Climatol.*, 35, 3132–3145, <https://doi.org/10.1002/joc.4198>, 2015.
- Asefi-Najafabady, S. and Saatchi, S.: Response of African humid tropical forests to recent rainfall anomalies., *Philos. Trans. R. Soc. B*, 368, 20120306, <https://doi.org/10.1098/rstb.2012.0306>, 2013.
- 645 Ashouri, H., Hsu, K. L., Sorooshian, S., Braithwaite, D. K., Knapp, K. R., Cecil, L. D., Nelson, B. R. and Prat, O. P.: PERSIANN-CDR: Daily precipitation climate data record from multisatellite observations for hydrological and climate studies, *Bull. Am. Meteorol. Soc.*, 96, 69–83, <https://doi.org/10.1175/BAMS-D-13-00068.1>, 2015.
- Awange, J. L., Ferreira, V. G., Forootan, E., Khandu, Andam-Akorful, S. A., Agutu, N. O. and He, X. F.: Uncertainties in remotely sensed precipitation data over Africa, *Int. J. Climatol.*, 36, 303–323, <https://doi.org/10.1002/joc.4346>, 2016.
- 650 Baldocchi, D., Wilson, K., Valentini, R., Law, B., Munger, W., Davis, K., Wofsy, S., Pilegaard, K., Goldstein, A., Falge, E., Vesala, T., Hollinger, D., Running, S., Fuentes, J., Katul, G., Gu, L., Verma, S., Paw, K. T., Malhi, Y., Anthoni, P., Oechel, W., Schmid, H. P., Bernhofer, C., Meyers, T., Evans, R., Olson, R. and Lee, X.: FLUXNET: A New Tool to Study the Temporal and Spatial Variability of Ecosystem–Scale Carbon Dioxide, Water Vapor, and Energy Flux Densities, *Bull. Am. Meteorol. Soc.*, 82, 2415–2434, <https://doi.org/10.1175/1520-0477>, 2002.
- 655 Balek, J., Ed.: *Hydrology and Water Resources in Tropical Africa*, *Dev. Water Res.*, 8, Elsevier, New York., 1977.
- Balek, J., Ed.: *Hydrology and Water Resources in Tropical Regions*, *Dev. Water Res.*, 18, Elsevier, New York., 1983.
- Batra, N., Yang, Y.-C. E., Choi, H. Il, Kumar, P., Cai, X. and De Fraiture, C.: Understanding Hydrological Cycle Dynamics Due to Changing Land Use and Land Cover: Congo Basin Case Study, in: *IEEE International Geoscience and Remote Sensing Symposium 2008 (IGARSS 2008)*, Boston, July 7-11 2008, V-491–V-494, <https://doi.org/10.1109/IGARSS.2008.4780136>, 2008.
- 660 Beighley, R. E., Ray, R. L., He, Y., Lee, H., Schaller, L., Andreadis, K. M., Durand, M., Alsdorf, D. E. and Shum, C. K.: Comparing satellite derived precipitation datasets using the Hillslope River Routing (HRR) model in the Congo River Basin, *Hydrol. Process.*, 25, 3216–3229, <https://doi.org/10.1002/hyp.8045>, 2011.
- 665 Bell, J. P., Tompkins, A. M., Bouka-Biona, C. and Sanda, I. S.: A process-based investigation into the impact of the Congo basin deforestation on surface climate, *J. Geophys. Res.*, 120, 5721–5739, <https://doi.org/10.1002/2014JD022586>, 2015.
- Betbeder, J., Gond, V., Frappart, F., Baghdadi, N. N., Briant, G. and Bartholome, E.: Mapping of Central Africa Forested Wetlands Using Remote Sensing, *IEEE J. Sel. Top. Appl. Earth Obs. Remote Sens.*, 7, 531–542, <https://doi.org/10.1109/JSTARS.2013.2269733>, 2014.
- 670 Bi, J., Myneni, R., Lyapustin, A., Wang, Y., Park, T., Chi, C., Yan, K. and Knyazikhin, Y.: Amazon forests’ response to droughts: A perspective from the MAIAC product, *Remote Sens.*, 8, 1–12, <https://doi.org/10.3390/rs8040356>, 2016.
- Brands, S., Herrera, S., Fernández, J. and Gutiérrez, J. M.: How well do CMIP5 Earth System Models simulate present climate



- conditions in Europe and Africa?, *Clim. Dyn.*, 41, 803–817, <https://doi.org/10.1007/s00382-013-1742-8>, 2013.
- Bricquet, J.-P.: Transports en solution et en suspension par le bassin du fleuve Congo, in: *Quatriemes Journees Hydrologiques de l'ORSTOM a Montpellier*, 131–161, ORSTOM, Montpellier, 1988.
- Bultot, F.: *Atlas Climatique du Bassin Congolais, Deuxieme Partie: Les Composantes du Bilan d'Eau*, L'Institut National pour L'Etude Agronomique du Congo (I.N.E.A.C.), Brussels, 1971.
- Chishugi, J. B. and Alemaw, B. F.: The Hydrology of the Congo River Basin: A GIS-based Hydrological Water Balance Model, in: *Proceedings of the 2009 World Environmental and Water Resources Congress: Great Rivers*, Kansas City, MO, May 17-21 2009, 5864–5879, 2009.
- Couralet, C., Van Den Bulcke, J., Ngoma, L. M., Van Acker, J. and Beeckman, H.: Phenology in functional groups of central african rainforest trees, *J. Trop. For. Sci.*, 25, 361–374, 2013.
- Crowhurst, D. M., Dadson, S. J. and Washington, R.: Evaluation of Evaporation Climatology for the Congo Basin Wet Seasons in Eleven Global Climate Models, *J. Geophys. Res. Atmos.*, <https://doi.org/10.1029/2019jd030619>, 2020.
- Crowley, J. W., Mitrovica, J. X., Bailey, R. C., Tamisiea, M. E. and Davis, J. L.: Land water storage within the Congo Basin inferred from GRACE satellite gravity data, *Geophys. Res. Lett.*, 33, L19402, <https://doi.org/10.1029/2006GL027070>, 2006.
- Cuthbert, M. O., Gleeson, T., Moosdorf, N., Befus, K. M., Schneider, A., Hartmann, J. and Lehner, B.: Global patterns and dynamics of climate–groundwater interactions, *Nat. Clim. Chang.*, 9, 137–141, <https://doi.org/10.1038/s41558-018-0386-4>, 2019.
- Dee, D. P., Uppala, S. M., Simmons, A. J., Berrisford, P., Poli, P., Kobayashi, S., Andrae, U., Balmaseda, M. A., Balsamo, G., Bauer, P., Bechtold, P., Beljaars, A. C. M., van de Berg, L., Bidlot, J., Bormann, N., Delsol, C., Dragani, R., Fuentes, M., Geer, A. J., Haimberger, L., Healy, S. B., Hersbach, H., Hólm, E. V., Isaksen, L., Kållberg, P., Köhler, M., Matricardi, M., McNally, A. P., Monge-Sanz, B. M., Morcrette, J. J., Park, B. K., Peubey, C., de Rosnay, P., Tavolato, C., Thépaut, J. N. and Vitart, F.: The ERA-Interim reanalysis: Configuration and performance of the data assimilation system, *Q. J. R. Meteorol. Soc.*, 137, 553–597, <https://doi.org/10.1002/qj.828>, 2011.
- Dembélé, M. and Zwart, S. J.: Evaluation and comparison of satellite-based rainfall products in Burkina Faso, West Africa, *Int. J. Remote Sens.*, 37, 3995–4014, <https://doi.org/10.1080/01431161.2016.1207258>, 2016.
- Dezfuli, A.: Climate of Western and Central Equatorial Africa, in: *Oxford Research Encyclopedia of Climate Science*, Oxford University Press, Oxford, <https://doi.org/10.1093/acrefore/9780190228620.013.511>, 2017.
- Diem, J. E., Ryan, S. J., Hartter, J. and Palace, M. W.: Satellite-based rainfall data reveal a recent drying trend in central equatorial Africa, *Clim. Change*, 126, 263–272, <https://doi.org/10.1007/s10584-014-1217-x>, 2014.
- Doelling, D.: CERES SYN1DEG-MONTH HDF4 file - Edition 4A, NASA Langley Atmospheric Science Data Center DAAC, https://doi.org/10.5067/TERRA+AQUA/CERES/SYN1DEGMONTH_L3.004A, 2017.
- Dyer, E. L. E., Jones, D. B. A., Nusbaumer, J., Li, H., Collins, O., Vettoretti, G. and Noone, D.: Congo Basin precipitation: Assessing seasonality, regional interactions, and sources of moisture, *J. Geophys. Res. Atmos.*, 122, 6882–6898, <https://doi.org/10.1002/2016JD026240>, 2017.



- Van Der Ent, R. J. and Savenije, H. H. G.: Length and time scales of atmospheric moisture recycling, *Atmos. Chem. Phys.*, 11, 1853–1863, <https://doi.org/10.5194/acp-11-1853-2011>, 2011.
- 710 Fisher, R. A., Williams, M., Do Vale, R. L., Da Costa, A. L. and Meir, P.: Evidence from Amazonian forests is consistent with isohydric control of leaf water potential, *Plant, Cell Environ.*, 29, 151–165, <https://doi.org/10.1111/j.1365-3040.2005.01407.x>, 2006.
- Friedl, M. and Sulla-Menashe, D.: MCD12C1 MODIS/Terra+Aqua Land Cover Type Yearly L3 Global 0.05Deg CMG V006, NASA Land Processes DAAC, <https://doi.org/10.5067/MODIS/MCD12C1.006>, 2015.
- 715 Funk, C., Peterson, P., Landsfeld, M., Pedreros, D., Verdin, J., Shukla, S., Husak, G., Rowland, J., Harrison, L., Hoell, A. and Michaelsen, J.: The climate hazards infrared precipitation with stations—a new environmental record for monitoring extremes, *Sci. Data*, 2, 150066, <https://doi.org/10.1038/sdata.2015.66>, 2015.
- Gelaro, R., McCarty, W., Suárez, M. J., Todling, R., Molod, A., Takacs, L., Randles, C. A., Darmenov, A., Bosilovich, M. G., Reichle, R., Wargan, K., Coy, L., Cullather, R., Draper, C., Akella, S., Buchard, V., Conaty, A., da Silva, A. M., Gu, W., Kim, G. K., Koster, R., Lucchesi, R., Merkova, D., Nielsen, J. E., Partyka, G., Pawson, S., Putman, W., Rienecker, M., Schubert, S. 720 D., Sienkiewicz, M. and Zhao, B.: The modern-era retrospective analysis for research and applications, version 2 (MERRA-2), *J. Clim.*, 30, 5419–5454, <https://doi.org/10.1175/JCLI-D-16-0758.1>, 2017.
- Guan, K., Wolf, A., Medvigy, D., Caylor, K. K., Pan, M. and Wood, E. F.: Seasonal coupling of canopy structure and function in African tropical forests and its environmental controls, *Ecosphere*, 4, <https://doi.org/10.1890/ES12-00232.1>, 2013.
- 725 Guan, K., Wood, E. F., Medvigy, D., Kimball, J., Pan, M., Caylor, K. K., Sheffield, J., Xu, X. and Jones, M. O.: Terrestrial hydrological controls on land surface phenology of African savannas and woodlands, *J. Geophys. Res. Biogeosciences*, 119, 1652–1669, <https://doi.org/10.1002/2013JG002572>, 2014.
- Guan, K., Pan, M., Li, H., Wolf, A., Wu, J., Medvigy, D., Caylor, K. K., Sheffield, J., Wood, E. F., Malhi, Y., Liang, M., Kimball, J. S., Saleska, S. R., Berry, J., Joiner, J. and Lyapustin, A. I.: Photosynthetic seasonality of global tropical forests constrained by hydroclimate, *Nat. Geosci.*, 8, 284–289, <https://doi.org/10.1038/ngeo2382>, 2015.
- 730 Guerrieri, R., Belmecheri, S., Ollinger, S. V., Asbjornsen, H., Jennings, K., Xiao, J., Stocker, B. D., Martin, M., Hollinger, D. Y., Bracho-Garrillo, R., Clark, K., Dore, S., Kolb, T., William Munger, J., Novick, K. and Richardson, A. D.: Disentangling the role of photosynthesis and stomatal conductance on rising forest water-use efficiency, *Proc. Natl. Acad. Sci. U. S. A.*, 116, 16909–16914, <https://doi.org/10.1073/pnas.1905912116>, 2019.
- Hassan, A. and Jin, S.: Water storage changes and balances in Africa observed by GRACE and hydrologic models, *Geod. Geodyn.*, 7, 39–49, <https://doi.org/10.1016/j.geog.2016.03.002>, 2016.
- 735 Hilker, T., Lyapustin, A. I., Tucker, C. J., Sellers, P. J., Hall, F. G. and Wang, Y.: Remote sensing of tropical ecosystems: Atmospheric correction and cloud masking matter, *Remote Sens. Environ.*, 127, 370–384, <https://doi.org/10.1016/j.rse.2012.08.035>, 2012.
- Hua, W., Zhou, L., Chen, H., Nicholson, S. E., Raghavendra, A. and Jiang, Y.: Possible causes of the Central Equatorial 740 African long-term drought, *Environ. Res. Lett.*, 11, <https://doi.org/10.1088/1748-9326/11/12/124002>, 2016.



- Hua, W., Zhou, L., Nicholson, S. E., Chen, H. and Qin, M.: Assessing reanalysis data for understanding rainfall climatology and variability over Central Equatorial Africa, *Clim. Dyn.*, 1–19, <https://doi.org/10.1007/s00382-018-04604-0>, 2019.
- Huete, A., Didan, K., Miura, T., Rodriguez, E. P., Gao, X. and Ferreira, L. G.: Overview of the radiometric and biophysical performance of the MODIS vegetation indices, *Remote Sens. Environ.*, 83, 195–213, 2002.
- 745 Huffman, G. J., Bolvin, D. T., Nelkin, E. J., Wolff, D. B., Adler, R. F., Gu, G., Hong, Y., Bowman, K. P. and Stocker, E. F.: The TRMM Multisatellite Precipitation Analysis (TMPA): Quasi-Global, Multiyear, Combined-Sensor Precipitation Estimates at Fine Scales, *J. Hydrometeorol.*, 8, 38–55, <https://doi.org/10.1175/JHM560.1>, 2007.
- James, R. and Washington, R.: Changes in African temperature and precipitation associated with degrees of global warming, *Clim. Change*, 117, 859–872, <https://doi.org/10.1007/s10584-012-0581-7>, 2013.
- 750 Jiang, Y., Zhou, L., Tucker, C. J., Raghavendra, A., Hua, W., Liu, Y. Y. and Joiner, J.: Widespread increase of boreal summer dry season length over the Congo rainforest, *Nat. Clim. Chang.*, 9, 617–622, <https://doi.org/10.1038/s41558-019-0512-y>, 2019.
- Joiner, J., Guanter, L., Lindstrot, R., Voigt, M., Vasilkov, A. P., Middleton, E. M., Huemmrich, K. F., Yoshida, Y. and Frankenberg, C.: Global monitoring of terrestrial chlorophyll fluorescence from moderate-spectral-resolution near-infrared satellite measurements: methodology, simulations, and application to GOME-2, *Atmos. Meas. Tech.*, 6, 2803–2823, <https://doi.org/10.5194/amt-6-2803-2013>, 2013.
- 755 Jung, M., Reichstein, M., Margolis, H. A., Cescatti, A., Richardson, A. D., Arain, M. A., Arneth, A., Bernhofer, C., Bonal, D., Chen, J., Gianelle, D., Gobron, N., Kiely, G., Kutsch, W., Lasslop, G., Law, B. E., Lindroth, A., Merbold, L., Montagnani, L., Moors, E. J., Papale, D., Sottocornola, M., Vaccari, F. and Williams, C.: Global patterns of land-atmosphere fluxes of carbon dioxide, latent heat, and sensible heat derived from eddy covariance, satellite, and meteorological observations, *J. Geophys. Res. Biogeosciences*, 116, 1–16, <https://doi.org/10.1029/2010JG001566>, 2011.
- 760 Jung, M., Koirala, S., Weber, U., Ichii, K., Gans, F., Camps-Valls, G., Papale, D., Schwalm, C., Tramontana, G. and Reichstein, M.: The FLUXCOM ensemble of global land-atmosphere energy fluxes, *Sci. Data*, 6, 74, <https://doi.org/10.1038/s41597-019-0076-8>, 2019.
- Kahn, B. H., Irion, F. W., Dang, V. T., Manning, E. M., Nasiri, S. L., Naud, C. M., Blaisdell, J. M., Schreier, M. M., Yue, Q., 765 Bowman, K. W., Fetzer, E. J., Hulley, G. C., Liou, K. N., Lubin, D., Ou, S. C., Susskind, J., Takano, Y., Tian, B. and Worden, J. R.: The atmospheric infrared sounder version 6 cloud products, *Atmos. Chem. Phys.*, 14, 399–426, <https://doi.org/10.5194/acp-14-399-2014>, 2014.
- Kanniah, K. D., Beringer, J. and Hutley, L.: Exploring the link between clouds, radiation, and canopy productivity of tropical savannas, *Agric. For. Meteorol.*, 182–183, 304–313, <https://doi.org/10.1016/j.agrformet.2013.06.010>, 2013.
- 770 De Kauwe, M. G., Medlyn, B. E., Zaehle, S., Walker, A. P., Dietze, M. C., Hickler, T., Jain, A. K., Luo, Y., Parton, W. J., Prentice, I. C., Smith, B., Thornton, P. E., Wang, S., Wang, Y. P., Wårlind, D., Weng, E., Crous, K. Y., Ellsworth, D. S., Hanson, P. J., Seok Kim, H., Warren, J. M., Oren, R. and Norby, R. J.: Forest water use and water use efficiency at elevated CO₂: A model-data intercomparison at two contrasting temperate forest FACE sites, *Glob. Chang. Biol.*, 19, 1759–1779, <https://doi.org/10.1111/gcb.12164>, 2013.



- 775 Keenan, T. F., Hollinger, D. Y., Bohrer, G., Dragoni, D., Munger, J. W., Schmid, H. P. and Richardson, A. D.: Increase in forest water-use efficiency as atmospheric carbon dioxide concentrations rise, *Nature*, 499, 324–327, <https://doi.org/10.1038/nature12291>, 2013.
- Konings, A. G. and Gentine, P.: Global variations in ecosystem-scale isohydricity, *Glob. Chang. Biol.*, 23, 891–905, <https://doi.org/10.1111/gcb.13389>, 2017.
- 780 Konings, A. G., Yu, Y., Xu, L., Yang, Y., Schimel, D. S. and Saatchi, S. S.: Active microwave observations of diurnal and seasonal variations of canopy water content across the humid African tropical forests, *Geophys. Res. Lett.*, 44, 2290–2299, <https://doi.org/10.1002/2016GL072388>, 2017.
- Landerer, F. W. and Swenson, S. C.: Accuracy of scaled GRACE terrestrial water storage estimates, *Water Resour. Res.*, 48, 1–11, <https://doi.org/10.1029/2011WR011453>, 2012.
- 785 Landerer, F. W., Dickey, J. O. and Güntner, A.: Terrestrial water budget of the Eurasian pan-Arctic from GRACE satellite measurements during 2003–2009, *J. Geophys. Res. Atmos.*, 115, 1–14, <https://doi.org/10.1029/2010JD014584>, 2010.
- Laporte, N. T., Stabach, J. A., Grosch, R., Lin, T. S. and Goetz, S. J.: Expansion of Industrial Logging in Central Africa, *Science*, 316, 1451, <https://doi.org/10.1126/science.1141057>, 2007.
- Lauer, W.: Climate and Weather, in: *Tropical Rain Forest Ecosystems: Biogeographical and Ecological Studies*, edited by H. Lieth and M. J. A. Werger, 7–53, Elsevier, New York., 1989.
- 790 Lee, H., Beighley, R. E., Alsdorf, D., Jung, H. C., Shum, C. K., Duan, J., Guo, J., Yamazaki, D. and Andreadis, K.: Characterization of terrestrial water dynamics in the Congo Basin using GRACE and satellite radar altimetry, *Remote Sens. Environ.*, 115, 3530–3538, <https://doi.org/10.1016/j.rse.2011.08.015>, 2011.
- Lehner, B., Verdin, K. and Jarvis, A.: New Global Hydrography Derived From Spaceborne Elevation Data, *Eos*, 89, 93–95, <https://doi.org/10.1029/2008EO100001>, 2008.
- 795 Lian, X., Piao, S., Huntingford, C., Li, Y., Zeng, Z., Wang, X., Ciais, P., McVicar, T. R., Peng, S., Ottlé, C., Yang, H., Yang, Y., Zhang, Y. and Wang, T.: Partitioning global land evapotranspiration using CMIP5 models constrained by observations, *Nat. Clim. Chang.*, 8, 640–646, <https://doi.org/10.1038/s41558-018-0207-9>, 2018.
- Liu, W., Wang, L., Zhou, J., Li, Y., Sun, F., Fu, G., Li, X. and Sang, Y. F.: A worldwide evaluation of basin-scale
800 evapotranspiration estimates against the water balance method, *J. Hydrol.*, 538, 82–95, <https://doi.org/10.1016/j.jhydrol.2016.04.006>, 2016.
- Loeb, N.: CERES Level 3B EBAF-Surface Terra+Aqua netCDF file - Edition 4.0, NASA Langley Atmospheric Science Data Center DAAC, https://doi.org/10.5067/TERRA+AQUA/CERES/EBAF-SURFACE_L3B004.0, 2017.
- Lorenz, C. and Kunstmann, H.: The Hydrological Cycle in Three State-of-the-Art Reanalyses: Intercomparison and
805 Performance Analysis, *J. Hydrometeorol.*, 13, 1397–1420, <https://doi.org/10.1175/JHM-D-11-088.1>, 2012.
- Lyapustin, A., Wang, Y., Korkin, S. and Huang, D.: MODIS Collection 6 MAIAC algorithm, *Atmos. Meas. Tech.*, 11, 5741–5765, <https://doi.org/10.5194/amt-11-5741-2018>, 2018.
- Lyapustin, A. I., Wang, Y., Laszlo, I., Hilker, T., G.Hall, F., Sellers, P. J., Tucker, C. J. and Korkin, S. V.: Multi-angle



- implementation of atmospheric correction for MODIS (MAIAC): 3. Atmospheric correction, *Remote Sens. Environ.*, 127,
810 385–393, <https://doi.org/10.1016/j.rse.2012.09.002>, 2012.
- Madani, N., Kimball, J. S., Parazoo, N. C., Ballantyne, A. P., Tagesson, T., Jones, L. A., Reichle, R. H., Palmer, P. I.,
Velicogna, I., Bloom, A. A., Saatchi, S., Liu, Z. and Geruo, A.: Below-surface water mediates the response of African forests
to reduced rainfall, *Environ. Res. Lett.*, 15, 034063, <https://doi.org/10.1088/1748-9326/ab724a>, 2020.
- Maeda, E. E., Moura, Y. M., Wagner, F., Hilker, T., Lyapustin, A. I., Wang, Y., Chave, J., Möttus, M., Aragão, L. E. O. C.
815 and Shimabukuro, Y.: Consistency of vegetation index seasonality across the Amazon rainforest, *Int. J. Appl. Earth Obs.*
Geoinf., 52, 42–53, <https://doi.org/10.1016/j.jag.2016.05.005>, 2016.
- Maeda, E. E., Ma, X., Wagner, F. H., Kim, H., Oki, T., Eamus, D. and Huete, A.: Evapotranspiration seasonality across the
Amazon Basin, *Earth Syst. Dyn.*, 8, 439–454, <https://doi.org/10.5194/esd-8-439-2017>, 2017.
- Marshall, M., Funk, C. and Michaelsen, J.: Examining evapotranspiration trends in Africa, *Clim. Dyn.*, 38, 1849–1865,
820 <https://doi.org/10.1007/s00382-012-1299-y>, 2012.
- Martens, B., Miralles, D. G., Lievens, H., Van Der Schalie, R., De Jeu, R. A. M., Fernández-Prieto, D., Beck, H. E., Dorigo,
W. A. and Verhoest, N. E. C.: GLEAM v3: Satellite-based land evaporation and root-zone soil moisture, *Geosci. Model Dev.*,
10, 1903–1925, <https://doi.org/10.5194/gmd-10-1903-2017>, 2017.
- Matsuyama, H., Oki, T., Shinoda, M. and Masuda, K.: The Seasonal Change of the Water Budget in the Congo River Basin,
825 *J. Meteorol. Soc. Japan*, 72, 281–299, 1994.
- McCull, K. A., Vogelzang, J., Konings, A. G., Entekhabi, D., Piles, M. and Stoffelen, A.: Extended triple collocation:
Estimating errors and correlation coefficients with respect to an unknown target, *Geophys. Res. Lett.*, 41, 6229–6236,
<https://doi.org/10.1002/2014GL061322>, 2014.
- McCollum, J. R., Gruber, A. and Ba, M. B.: Discrepancy between Gauges and Satellite Estimates of Rainfall in Equatorial
830 Africa, *J. Appl. Meteorol.*, 39, 666–679, <https://doi.org/10.1175/1520-0450-39.5.666>, 2000.
- Mercado, L. M., Bellouin, N., Sitch, S., Boucher, O., Huntingford, C., Wild, M. and Cox, P. M.: Impact of changes in diffuse
radiation on the global land carbon sink, *Nature*, 458, 1014–1017, <https://doi.org/10.1038/nature07949>, 2009.
- Met Office: Met Office Integrated Data Archive System (MIDAS) Land and Marine Surface Station Data (1853-current),
NCAS British Atmospheric Data Centre, available at:
835 <http://catalogue.ceda.ac.uk/uuid/220a65615218d5c9cc9e4785a3234bd0>, 2012.
- Miralles, D. G., Holmes, T. R. H., De Jeu, R. A. M., Gash, J. H., Meesters, A. G. C. A. and Dolman, A. J.: Global land-surface
evaporation estimated from satellite-based observations, *Hydrol. Earth Syst. Sci.*, 15, 453–469, <https://doi.org/10.5194/hess-15-453-2011>, 2011.
- Mu, Q., Zhao, M. and Running, S. W.: MODIS Global Terrestrial Evapotranspiration (ET) Product (MOD16A2/A3):
840 Algorithm Theoretical Basis Document, University of Montana, Missoula, MT, 55 pp., 2013.
- Müller, R., Pfeifroth, U., Träger-Chatterjee, C., Trentmann, J. and Cremer, R.: Digging the METEOSAT treasure—3 decades
of solar surface radiation, *Remote Sens.*, 7, 8067–8101, <https://doi.org/10.3390/rs70608067>, 2015.



- Munzimi, Y. A., Hansen, M. C., Adusei, B. and Senay, G. B.: Characterizing Congo basin rainfall and climate using Tropical Rainfall Measuring Mission (TRMM) satellite data and limited rain gauge ground observations, *J. Appl. Meteorol. Climatol.*, 845 54, 541–555, <https://doi.org/10.1175/JAMC-D-14-0052.1>, 2015.
- Ndehedehe, C. E., Okwuashi, O., Ferreira, V. G. and Agutu, N. O.: Exploring evapotranspiration dynamics over Sub-Sahara Africa (2000–2014), *Environ. Monit. Assess.*, 190, <https://doi.org/10.1007/s10661-018-6780-6>, 2018.
- Nguyen, P., Ombadi, M., Sorooshian, S., Hsu, K., AghaKouchak, A., Brathwaite, D., Ashouri, H. and Thorstensen, A. R.: The PERSIANN Family of Global Satellite Precipitation Data: A Review and Evaluation of Products, *Hydrol. Earth Syst. Sci. Discuss.*, 1–34, <https://doi.org/10.5194/hess-2018-177>, 2018.
- Nicholson, S. E., Kim, J., Ba, M. B. and Lare, A. R.: The mean surface water balance over Africa and its interannual variability, *J. Clim.*, 10, 2981–3002, [https://doi.org/10.1175/1520-0442\(1997\)010<2981:TMSWBO>2.0.CO;2](https://doi.org/10.1175/1520-0442(1997)010<2981:TMSWBO>2.0.CO;2), 1997.
- Nicholson, S. E., Klotter, D., Dezfuli, A. K. and Zhou, L.: New Rainfall Datasets for the Congo Basin and Surrounding Regions, *J. Hydrometeorol.*, 19, 1379–1396, <https://doi.org/10.1175/JHM-D-18-0015.1>, 2018.
- 855 Nicholson, S. E., Klotter, D., Zhou, L. and Hua, W.: Validation of Satellite Precipitation Estimates over the Congo Basin, *J. Hydrometeorol.*, 20, 631–656, <https://doi.org/10.1175/JHM-D-18-0118.1>, 2019.
- Nizinski, J. J., Galat, G. and Galat-Luong, A.: Water balance and sustainability of eucalyptus plantations in the Kouilou basin (Congo-Brazzaville), *Russ. J. Ecol.*, 42, 305–314, <https://doi.org/10.1134/S1067413611040126>, 2011.
- Nizinski, J. J., Galat, G. and Galat-Luong, A.: Actual evapotranspiration and canopy resistance measurement of the savannah 860 in the Kouilou basin (Congo-Brazzaville), *Russ. J. Ecol.*, 45, 359–366, <https://doi.org/10.1134/S1067413614050191>, 2014.
- Oki, T., Musiakke, K., Masuda, K. and Matsuyama, H.: Global runoff estimation by atmospheric water balance using ECMWF data set, in: *Proceedings of the IAHS Yokohama Symposium: Hydrology of Warm Humid Regions*, Yokohama, Japan, July 13-15 1993, 163–171, 1993.
- Olivry, J. C., Bricquet, J. P. and Mahé, G.: Vers un appauvrissement durable des ressources en eau de l’Afrique humide?, in: 865 *Proceedings of the IAHS Yokohama Symposium: Hydrology of Warm Humid Regions*, Yokohama, Japan, July 13-15 1993, 67–78, 1993.
- Opoku-Duah, S., Donoghue, D. N. M. and Burt, T. P.: Intercomparison of evapotranspiration over the Savannah Volta Basin in West Africa using remote sensing data, *Sensors*, 8, 2736–2761, <https://doi.org/10.3390/s8042736>, 2008.
- Pan, M., Sahoo, A. K., Troy, T. J., Vinukollu, R. K., Sheffield, J. and Wood, A. E. F.: Multisource estimation of long-term 870 terrestrial water budget for major global river basins, *J. Clim.*, 25, 3191–3206, <https://doi.org/10.1175/JCLI-D-11-00300.1>, 2012.
- Peñuelas, J., Canadell, J. G. and Ogaya, R.: Increased water-use efficiency during the 20th century did not translate into enhanced tree growth, *Glob. Ecol. Biogeogr.*, 20, 597–608, <https://doi.org/10.1111/j.1466-8238.2010.00608.x>, 2011.
- Philippon, N., de Lapparent, B., Gond, V., Sèze, G., Martiny, N., Camberlin, P., Cornu, G., Morel, B., Moron, V., Bigot, S., 875 Brou, T. and Dubreuil, V.: Analysis of the diurnal cycles for a better understanding of the mean annual cycle of forests greenness in Central Africa, *Agric. For. Meteorol.*, 223, 81–94, <https://doi.org/10.1016/j.agrformet.2016.04.005>, 2016.



- Philippon, N., Cornu, G., Monteil, L., Gond, V., Moron, V., Pergaud, J., Sèze, G., Bigot, S., Camberlin, P., Doumenge, C., Fayolle, A. and Ngomanda, A.: The light-deficient climates of western Central African evergreen forests, *Environ. Res. Lett.*, 14, 034007, <https://doi.org/10.1088/1748-9326/aaf5d8>, 2019.
- 880 Pinet, P. and Souriau, M.: Continental erosion and large-scale relief, *Tectonics*, 7, 563–582, <https://doi.org/10.1029/TC007i003p00563>, 1988.
- Pokam, W. M., Djotang, L. A. T. and Mkankam, F. K.: Atmospheric water vapor transport and recycling in Equatorial Central Africa through NCEP/NCAR reanalysis data, *Clim. Dyn.*, 38, 1715–1729, <https://doi.org/10.1007/s00382-011-1242-7>, 2012.
- Rocha, A. V., Su, H. B., Vogel, C. S., Schmid, H. P. and Curtis, P. S.: Photosynthetic and water use efficiency responses to
885 diffuse radiation by an aspen-dominated northern hardwood forest, *For. Sci.*, 50, 793–801, 2004.
- Rodell, M., Famiglietti, J. S., Chen, J., Seneviratne, S. I., Viterbo, P., Holl, S. and Wilson, C. R.: Basin scale estimates of evapotranspiration using GRACE and other observations, *Geophys. Res. Lett.*, 31, 10–13, <https://doi.org/10.1029/2004GL020873>, 2004a.
- Rodell, M., Famiglietti, J. S., Wiese, D. N., Reager, J. T., Beaulieu, H. K., Landerer, F. W. and Lo, M. H.: Emerging trends
890 in global freshwater availability, *Nature*, 557, 651–659, <https://doi.org/10.1038/s41586-018-0123-1>, 2018.
- Rodell, M., Houser, P. R., Jambor, U., Gottschalck, J., Mitchell, K., Meng, C., Arsenault, K., Cosgrove, B., Radakovich, J., Bosilovich, M., Entin, J. K., Walker, J. P., Lohmann, D. and Toll, D.: The Global Land Data Assimilation System, *Bull. Am. Meteorol. Soc.*, 85, 381–394, <https://doi.org/10.1175/BAMS-85-3-381>, 2004b.
- Rodell, M., McWilliams, E. B., Famiglietti, J. S., Beaulieu, H. K. and Nigro, J.: Estimating evapotranspiration using an
895 observation based terrestrial water budget, *Hydrol. Process.*, 25, 4082–4092, <https://doi.org/10.1002/hyp.8369>, 2011.
- Russell, G. L. and Miller, J. R.: Global River Runoff Calculated from a Global Atmospheric General Circulation Model, *J. Hydrol.*, 117, 241–254, 1990.
- Ryu, Y., Jiang, C., Kobayashi, H. and Detto, M.: MODIS-derived global land products of shortwave radiation and diffuse and total photosynthetically active radiation at 5 km resolution from 2000, *Remote Sens. Environ.*, 204, 812–825,
900 <https://doi.org/10.1016/j.rse.2017.09.021>, 2018.
- Saeed, F., Haensler, A., Weber, T., Hagemann, S. and Jacob, D.: Representation of extreme precipitation events leading to opposite climate change signals over the Congo basin, *Atmosphere-Basel*, 4, 254–271, <https://doi.org/10.3390/atmos4030254>, 2013.
- Sakumura, C., Bettadpur, S. and Bruinsma, S.: Ensemble prediction and intercomparison analysis of GRACE time-variable
905 gravity field models, *Geophys. Res. Lett.*, 41, 1389–1397, <https://doi.org/10.1002/2013GL058632>, 2014.
- Schneider, U., Becker, A., Finger, P., Meyer-Christoffer, A., Rudolf, B. and Ziese, M.: GPCC Full Data Monthly Product Version 7.0 at 2.5°: Monthly Land-Surface Precipitation from Rain-Gauges built on GTS-based and Historic Data, Global Precipitation Climatology Centre (GPCC), https://doi.org/10.5676/DWD_GPCC/FD_M_V7_250, 2015.
- Schüttemeyer, D., Schillings, C., Moene, A. F. and de Bruin, H. A. R.: Satellite-based actual evapotranspiration over drying
910 semiarid terrain in West Africa, *J. Appl. Meteorol. Climatol.*, 46, 97–111, <https://doi.org/10.1175/JAM2444.1>, 2007.



- Shahin, M.: Evapotranspiration, in: *Hydrology and Water Resources of Africa*, 157–212, Springer Netherlands, Dordrecht, 1994.
- Shem, W. O.: Biosphere-atmosphere interaction over the Congo Basin and its influence on the regional hydrological cycle, Ph.D. thesis, School of Earth and Atmospheric Sciences, Georgia Institute of Technology, USA, 141 pp., 2006.
- 915 Shirke, P. A.: Leaf photosynthesis, dark respiration, and fluorescence as influenced by leaf age in an evergreen tree, *Prosopis juliflora*, *Photosynthetica*, 39, 305–311, <https://doi.org/10.1023/A:1013761410734>, 2001.
- Van Der Sleen, P., Groenendijk, P., Vlam, M., Anten, N. P. R., Boom, A., Bongers, F., Pons, T. L., Terburg, G. and Zuidema, P. A.: No growth stimulation of tropical trees by 150 years of CO₂ fertilization but water-use efficiency increased, *Nat. Geosci.*, 8, 24–28, <https://doi.org/10.1038/ngeo2313>, 2015.
- 920 Sobrado, M. A.: Leaf age effects on photosynthetic rate, transpiration rate and nitrogen content in a tropical dry forest, *Physiol. Plant.*, 90, 210–215, <https://doi.org/10.1111/j.1399-3054.1994.tb02213.x>, 1994.
- Sorí, R., Nieto, R., Vicente-Serrano, S. M., Drumond, A. and Gimeno, L.: A Lagrangian perspective of the hydrological cycle in the Congo River basin, *Earth Syst. Dyn.*, 8, 653–675, <https://doi.org/10.5194/esd-8-653-2017>, 2017.
- Stoffelen, A.: Toward the true near-surface wind speed: Error modeling and calibration using triple collocation, *J. Geophys. Res. Ocean.*, 103, 7755–7766, <https://doi.org/10.1029/97JC03180>, 1998.
- 925 Swann, A. L. S. and Koven, C. D.: A Direct Estimate of the Seasonal Cycle of Evapotranspiration over the Amazon Basin, *J. Hydrometeorol.*, 18, 2173–2185, <https://doi.org/10.1175/JHM-D-17-0004.1>, 2017.
- Swenson, S. and Wahr, J.: Post-processing removal of correlated errors in GRACE data, *Geophys. Res. Lett.*, 33, 1–4, <https://doi.org/10.1029/2005GL025285>, 2006.
- 930 Swenson, S. C.: GRACE MONTHLY LAND WATER MASS GRIDS NETCDF RELEASE Ver. 5.0, NASA Physical Oceanography DAAC, <https://doi.org/10.5067/TELND-NC005>, 2012.
- Tapley, B. D., Bettadpur, S., Ries, J. C., Thompson, P. F. and Watkins, M. M.: GRACE Measurements of Mass Variability in the Earth System, *Science*, 305, 503–505, <https://doi.org/10.1126/science.1099192>, 2004.
- Taylor, K. E.: Summarizing multiple aspects of model performance in a single diagram, *J. Geophys. Res.*, 106, 7183–7192, 935 2001.
- Thiemig, V., Rojas, R., Zambrano-Bigiarini, M., Levizzani, V. and De Roo, A.: Validation of Satellite-Based Precipitation Products over Sparsely Gauged African River Basins, *J. Hydrometeorol.*, 13, 1760–1783, <https://doi.org/10.1175/JHM-D-12-032.1>, 2012.
- Turubanova, S., Potapov, P. V., Tyukavina, A. and Hansen, M. C.: Ongoing primary forest loss in Brazil, Democratic Republic of the Congo, and Indonesia, *Environ. Res. Lett.*, 13, <https://doi.org/10.1088/1748-9326/aacd1c>, 2018.
- 940 Ukkola, A. M. and Prentice, I. C.: A worldwide analysis of trends in water-balance evapotranspiration, *Hydrol. Earth Syst. Sci.*, 17, 4177–4187, <https://doi.org/10.5194/hess-17-4177-2013>, 2013.
- Urban, J., Ingwers, M. W., McGuire, M. A. and Teskey, R. O.: Increase in leaf temperature opens stomata and decouples net photosynthesis from stomatal conductance in *Pinus taeda* and *Populus deltoides* x *nigra*, *J. Exp. Bot.*, 68, 1757–1767,



- 945 <https://doi.org/10.1093/jxb/erx052>, 2017.
Verbesselt, J., Hyndman, R., Newnham, G. and Culvenor, D.: Detecting trend and seasonal changes in satellite image time series, *Remote Sens. Environ.*, 114, 106–115, <https://doi.org/10.1016/j.rse.2009.08.014>, 2010a.
Verbesselt, J., Hyndman, R., Zeileis, A. and Culvenor, D.: Phenological change detection while accounting for abrupt and gradual trends in satellite image time series, *Remote Sens. Environ.*, 114, 2970–2980,
950 <https://doi.org/10.1016/j.rse.2010.08.003>, 2010b.
Verbesselt, J., Zeileis, A. and Hyndman, R.: Breaks for Additive Season and Trend (BFAST), available at: <http://bfast.r-forge.r-project.org>, 2015.
Vinya, R., Malhi, Y., Brown, N. D., Fisher, J. B., Brodribb, T. and Aragão, L. E. O. C.: Seasonal changes in plant–water relations influence patterns of leaf display in Miombo woodlands: evidence of water conservative strategies, *Tree Physiol.*, 39,
955 104–112, <https://doi.org/10.1093/treephys/tpy062>, 2019.
Wahr, J., Swenson, S. and Velicogna, I.: Accuracy of GRACE mass estimates, *Geophys. Res. Lett.*, 33, 1–5, <https://doi.org/10.1029/2005GL025305>, 2006.
Wan, Z., Zhang, K., Xue, X., Hong, Z., Hong, Y. and Gourley, J. J.: Water balance-based actual evapotranspiration reconstruction from ground and satellite observations over the conterminous United States, *Water Resour. Res.*, 51, 6485–
960 6499, <https://doi.org/10.1002/2015WR017311>, 2015.
Washington, R., James, R., Pearce, H., Pokam, W. M. and Moufouma-Okia, W.: Congo Basin rainfall climatology: can we believe the climate models?, *Philos. Trans. R. Soc. B Biol. Sci.*, 368, 1–7, <https://doi.org/10.1098/rstb.2012.0296>, 2013.
Weerasinghe, I., Bastiaanssen, W., Mul, M., Jia, L. and van Griensven, A.: Can we trust remote sensing evapotranspiration products over Africa?, *Hydrol. Earth Syst. Sci.*, 24, 1565–1586, <https://doi.org/10.5194/hess-24-1565-2020>, 2020.
965 Wu, J., Albert, L. P., Lopes, A. P., Restrepo-Coupe, N., Hayek, M., Wiedemann, K. T., Guan, K., Stark, S. C., Christoffersen, B., Prohaska, N., Tavares, J. V., Marostica, S., Kobayashi, H., Ferreira, M. L., Campos, K. S., da Silva, R., Brando, P. M., Dye, D. G., Huxman, T. E., Huete, A. R., Nelson, B. W. and Saleska, S. R.: Leaf development and demography explain photosynthetic seasonality in Amazon evergreen forests, *Science*, 351, 972–976, <https://doi.org/10.1126/science.aad5068>, 2016.
970 Yin, X. and Gruber, A.: Validation of the abrupt change in GPCP precipitation in the Congo River Basin, *Int. J. Climatol.*, 30, 110–119, <https://doi.org/10.1002/joc.1875>, 2010.
Yuan, W., Zheng, Y., Piao, S., Ciais, P., Lombardozzi, D., Wang, Y., Ryu, Y., Chen, G., Dong, W., Hu, Z., Jain, A. K., Jiang, C., Kato, E., Li, S., Lienert, S., Liu, S., Nabel, J. E. M. S., Qin, Z., Quine, T., Sitch, S., Smith, W. K., Wang, F., Wu, C., Xiao, Z. and Yang, S.: Increased atmospheric vapor pressure deficit reduces global vegetation growth, *Sci. Adv.*, 5, 1–12,
975 <https://doi.org/10.1126/sciadv.aax1396>, 2019.
Zhang, K., Kimball, J. S. and Running, S. W.: A review of remote sensing based actual evapotranspiration estimation, *Wiley Interdiscip. Rev. Water*, 3, 834–853, <https://doi.org/10.1002/wat2.1168>, 2016.
Zhang, Y., Joiner, J., Gentine, P. and Zhou, S.: Reduced solar-induced chlorophyll fluorescence from GOME-2 during Amazon



drought caused by dataset artifacts, *Glob. Chang. Biol.*, 24, 2229–2230, <https://doi.org/10.1111/gcb.14134>, 2018.

980 Zhou, L., Tian, Y., Myneni, R. B., Ciais, P., Saatchi, S., Liu, Y. Y., Piao, S., Chen, H., Vermote, E. F., Song, C. and Hwang, T.: Widespread decline of Congo rainforest greenness in the past decade, *Nature*, 508, 86–90, <https://doi.org/10.1038/nature13265>, 2014.